Dalton Transactions

PAPER

View Article Online
View Journal | View Issue

Cite this: *Dalton Trans.*, 2016, **45**, 8916

Thermodynamic description of Tc(IV) solubility and hydrolysis in dilute to concentrated NaCl, $MgCl_2$ and $CaCl_2$ solutions†

Ezgi Yalçıntaş,* Xavier Gaona,* Marcus Altmaier, Kathy Dardenne, Robert Polly and Horst Geckeis

We present the first systematic investigation of Tc(IV) solubility, hydrolysis and speciation in dilute to concentrated NaCl, $MgCl_2$ and $CaCl_2$ systems, and comprehensive thermodynamic and activity models for the system Tc^{4+}–H^+–Na^+–Mg^{2+}–Ca^{2+}–OH^-–Cl^-–H_2O using both SIT and Pitzer approaches. The results are advancing the fundamental scientific understanding of Tc(IV) solution chemistry and are highly relevant in the applied context of nuclear waste disposal. The solubility of Tc(IV) was investigated in carbonate-free NaCl–NaOH (0.1–5.0 M), $MgCl_2$ (0.25–4.5 M) and $CaCl_2$ (0.25–4.5 M) solutions within $2 \leq pH_m \leq 14.5$. Undersaturation solubility experiments were performed under an Ar atmosphere at $T = 22 \pm 2$ °C. Strongly reducing conditions (pe + $pH_m \leq 2$) were imposed with $Na_2S_2O_4$, $SnCl_2$ and Fe powder to stabilize technetium in the +IV redox state. The predominance of Tc(IV) in the aqueous phase was confirmed by solvent extraction and XANES/EXAFS spectroscopy. Solid phase characterization was accomplished after attaining thermodynamic equilibrium using XRD, SEM–EDS, XANES/EXAFS, TG–DTA and quantitative chemical analysis, and indicated that $TcO_2{\cdot}0.6H_2O$(s) exerts solubility-control in all evaluated systems. The definition of the polyatomic $Tc_3O_5^{2+}$ species instead of TcO^{2+} is favoured under acidic conditions, consistently with slope analysis (m_{Tc} *vs.* pH_m) of the solubility data gained in this work and spectroscopic evidence previously reported in the literature. The additional formation of Tc(IV)–OH/O–Cl aqueous species in concentrated chloride media ($[Cl^-]$ = 9 M) and $pH_m \leq 4$ is suggested by solubility and EXAFS data. The pH-independent behaviour of the solubility observed under weakly acidic to weakly alkaline pH_m conditions can be explained with the equilibrium reaction $TcO_2{\cdot}0.6H_2O(s) + 0.4H_2O(l) \Leftrightarrow TcO(OH)_2(aq)$. Solubility data determined in dilute NaCl systems with $pH_m \geq 11$ follow a well-defined slope of +1, consistent with the predominance of $TcO(OH)_3^-$ previously selected by NEA–TDB. In concentrated $MgCl_2$ and $CaCl_2$ solutions with $pH_m \geq 8$, the formation of the ternary $Mg_3[TcO(OH)_5]^{3+}$ and $Ca_3[TcO(OH)_5]^{3+}$ species is proposed based on the slope analysis of the solubility data, model calculations and previous observations for analogous An(IV) and Zr(IV) systems. The formation and stability of these hitherto unknown Tc(IV) species are supported by DFT calculations. Based on the newly generated experimental data and previous spectroscopic observations, new comprehensive chemical, thermodynamic and activity models (SIT, Pitzer) for these systems are derived.

Received 11th March 2016,
Accepted 16th April 2016

DOI: 10.1039/c6dt00973e

www.rsc.org/dalton

1 Introduction

^{99}Tc is a fission product of ^{235}U and ^{239}Pu forming with a high yield in nuclear reactors. The behaviour of ^{99}Tc in repositories for radioactive waste needs to be properly assessed due to its redox sensitive character, very long half-life ($t_{1/2} \sim 2.13 \times 10^5$ a) and potential contribution to the dose rate of radioactive waste in the long-term. Two main oxidation states of Tc (+VII and +IV) control the potential release and migration of this radionuclide from the repository into the biosphere. Tc(VII) is the most stable oxidation state in suboxic/oxidizing environments, forming the highly mobile TcO_4^- anion over the entire pH range with very high solubility and very weak sorption properties.[1] In contrast, Tc(IV) forms sparingly soluble oxides $TcO_2{\cdot}xH_2O$(s) under reducing conditions, and thus it is expected to control the chemical behaviour of Tc under the redox conditions expected in deep underground repositories for radioactive waste.

Institute for Nuclear Waste Disposal, Karlsruhe Institute of Technology, P.O. Box 3640, 76021 Karlsruhe, Germany. E-mail: ezgi.yalcintas@kit.edu, xavier.gaona@kit.edu

†Electronic supplementary information (ESI) available. See DOI: 10.1039/c6dt00973e

The geochemical conditions in underground repositories are mostly defined by the host-rock formation, composition of the groundwater, backfill material, waste inventories and waste form, among others. Although dilute conditions ($I < 0.1$ M) are normally expected for intruding waters in clay and crystalline host-rock formations, high saline (5 M < I < 15 M) systems are expected in certain sedimentary rocks and salt-rock formations. The latter systems are characterized by high concentrations of Na^+, Mg^{2+}, K^+, Cl^- and SO_4^{2-} with lower contributions of Ca^{2+}, HCO_3^-, F^- and Br^-.[2] The use of cement-based materials for conditioning/stabilization of the waste or construction purposes in a repository potentially leads to an alteration of the geochemical media buffering the pH in the hyperalkaline range and inducing a significant increase in the Ca concentration (≈ 0.02 M at pH ≈ 12.5).[3] In concentrated salt brine systems, the interaction of $MgCl_2$ with cement can further lead to the formation of concentrated $CaCl_2$ systems (up to 2.0 M) with $pH_m \approx 12$ ($pH_m = -\log m_{H^+}$).[4] The solution chemistry of radionuclides in saline systems of high ionic strength cannot be predicted from data and model descriptions gained in dilute systems, mainly because of strong ion interaction processes taking place in the former, leading to a potential strong stabilisation or de-stabilisation of species in brine systems. Besides ion interaction processes which may significantly affect the chemical behaviour and thermodynamic equilibria, the presence of high concentrations of cations like Mg^{2+} or Ca^{2+} can further result in the formation of new aqueous species or solid compounds not observed in dilute systems. Apart from being an interesting research topic from the perspective of fundamental aquatic chemistry, this tendency can lead to completely different chemical properties and migration behaviour of radionuclides in salt brine systems, which therefore justifies dedicated research efforts.

The solubility of Tc(IV) was previously investigated by a number of research groups, in most of the cases at low ionic strength. Meyer *et al.*[5] studied the solubility of Tc(IV) in the pH range 1 to 10. Two different approaches were used for the preparation of the solid phase, namely electrodeposition of an oxide solid phase and the oxide precipitation onto sand particles from reduction of Tc(VII) by hydrazine. The authors determined the number of hydration waters in $TcO_2{\cdot}xH_2O$(s) as (1.63 ± 0.28) by weighing the dried solid phases reduced under acidic and alkaline conditions. Based on their solubility data, Meyer and co-workers proposed a chemical model with TcO^{2+} and $TcO(OH)^+$ species prevailing under acidic conditions. On the other hand, the chemical equilibrium $TcO_2{\cdot}1.6H_2O(s) \Leftrightarrow TcO(OH)_2(aq) + 0.6H_2O(l)$ was proposed to explain the very low and pH-independent solubility behaviour within $4 \leq pH \leq 10$. Eriksen *et al.*[6] performed solubility experiments with an electrodeposited Tc(IV) oxide as a function of pH and P_{CO_2}. Consistently with Meyer and co-workers, these authors observed a pH-independent solubility ($\approx 7 \times 10^{-9}$ M) within the pH range 6 to 9.5. The increase in solubility with slope +1 observed above pH = 9.5 was interpreted as the formation of the $TcO(OH)_3^-$ species in accordance with the chemical reaction $TcO_2{\cdot}xH_2O(s) \Leftrightarrow TcO(OH)_3^- + H^+ + (x - 2)H_2O(l)$ and $\log K^\circ_{s,TcO(OH)_3^-} = -(19.2 \pm 0.3)$. Hess *et al.* (2004)[7] conducted solubility experiments in dilute to concentrated saline systems (up to 5.0 M NaCl and 6.0 M HCl) under acidic to near-neutral pH conditions. Samples were equilibrated for up to 65 days. The solubility study was complemented with extensive solid and aqueous phase characterization, including XRD, UV-vis, XANES/EXAFS and liquid–liquid extraction. In spite of the high [Cl^-] considered in the study, the authors only reported evidence on the formation of Tc(IV)–Cl species ($TcCl_4$(aq) and $TcCl_6^{2-}$) at $pH_m \leq 1$ and $I \geq 2.5$ M. The transformation of $TcO_2{\cdot}xH_2O$(s) to $TcCl_4$(s) was also proposed to take place under these conditions. Above $pH_m \approx 1$, Hess and co-workers reported the predominance of Tc(IV) hydrolysis species and explained the significant increase in solubility observed in concentrated NaCl solutions exclusively by ion interaction processes. The authors derived comprehensive chemical, thermodynamic and activity models for Tc(IV) in acidic HCl–NaCl systems based on their solubility data at short equilibration times (t = 11 days) and the corresponding solid and aqueous phase characterization. The chemical model reported by Hess *et al.* is in agreement with previous publications available in the literature and with the current NEA–TDB data selection, although the authors reported greater $\log K^\circ_{s,TcO(OH)^+}$ for the $TcO(OH)^+$ species, which accordingly becomes predominant in the acidic pH region. Later, Liu *et al.* (2007)[8] performed Tc(IV) solubility experiments in simulated ground water within $1 \leq pH \leq 12$ and 10^{-4} M $\leq [CO_3^{2-}] \leq 0.05$ M. The authors found a good agreement with previous publications and did not observe any relevant increase in Tc(IV) solubility due to carbonate complexation. Warwick *et al.*[9] investigated the solubility of Tc(IV) reduced by Sn(II) and Fe(II) within the pH range 11.8 to 14.4. In contrast to the solubility data by Eriksen and co-workers, the authors only observed a slight increase of Tc(IV) solubility above pH = 13.5. Unfortunately, no solid phase characterization was conducted by the authors, and thus it can only be speculated that a more crystalline solid or alteration phase was eventually responsible for the control of the solubility in this study. Kobayashi and co-workers (2013)[10] investigated the reduction of Tc(VII) to Tc(IV) in 0.1 M NaCl and the presence of various reducing systems. The authors compared their experimental results with thermodynamic calculations of the Tc(VII)/Tc(IV) redox border, with the aim of assessing the kinetics of the reduction process and the reliability of E_h–pH measurements. Recently, Yalcintas *et al.*[11] extended the redox experiments by Kobayashi *et al.* to dilute and concentrated NaCl and $MgCl_2$ solutions in order to evaluate the effect of elevated ionic strength on the redox behaviour of Tc. Besides the impact of salt concentration on the measured E_h values, a systematic increase in the concentration of Tc(IV) under acidic conditions was observed with increasing ionic strength, thus reflecting a relevant impact of ion interaction processes on the aquatic chemistry of Tc(IV).

Besides these studies specifically targeting the determination of thermodynamic data, a number of spectroscopic investigations providing relevant insights into the speciation of Tc under acidic conditions have been published since

2000.[12–16] Hence, Vichot *et al.* (2002) investigated the speciation of Tc(IV) in aqueous Cl^- and SO_4^{2-} media at pH ≈ 1.5 and $I \leq 3$ M.[12] Based on the evaluation of their EXAFS data, the authors proposed the formation of small sized polynuclear species independently of the composition of the background electrolyte. EXAFS data disregarded also the presence of Cl backscatterers in the first coordination shell of Tc. In 2003, the same authors confirmed the formation and predominance of polymeric $Tc_nO_p^{(4n-2p)+}$ species up to pH = 3 using UV-vis spectroscopy, clearly contradicting the previously postulated predominance of the monomeric TcO^{2+} and $TcO(OH)^+$ species. The authors interpreted their data with the formation of the trimer $Tc_3O_4^{4+}$, which shows clear analogies with the cluster $M_3O_4{\cdot}9H_2O^{4+}$ previously described for Mo(IV).[13] Poineau *et al.* (2006)[16] investigated the aqueous speciation of Tc in 3.0 M HCl–NaCl solutions with $0 \leq pH \leq 1.5$ using a combination of spectroscopic techniques (UV-vis/NIR and EXAFS). The authors confirmed the predominance of the $Tc_2OCl_{10}^{4-}$ species at $0.1 \leq pH \leq 1.1$, whereas $TcCl_6^{2-}$ and $Tc_nO_p^{(4n-2p)+}$ prevailed below and above this pH range, respectively.[17]

In spite of the abundant experimental studies focussing on the aquatic chemistry of Tc(IV), a number of open questions remain with regard to the chemical and thermodynamic models available for this system. Furthermore, the lack of systematic studies at elevated ionic strength hinders the development of accurate activity models able to predict the chemical behaviour of Tc(IV) at $I \neq 0$ and directly impacts the possibilities to model Tc chemistry in salt media. In this context, the present study aims at a comprehensive and systematic investigation of Tc(IV) solubility and hydrolysis in dilute to concentrated NaCl, $MgCl_2$ and $CaCl_2$ systems relevant for different nuclear waste disposal concepts and scenarios. Solubility experiments are complemented with comprehensive solid and aqueous phase characterisation contributing to the development of an accurate chemical model for this system. The thermodynamic and activity models for the system Tc^{4+}–H^+–Na^+–Mg^{2+}–Ca^{2+}–OH^-–Cl^-–H_2O are derived based on the newly generated experimental data using SIT and Pitzer approaches.

1.1. Thermodynamic background

1.1.1 Current NEA–TDB selection for Tc. The thermochemical database project of the Nuclear Energy Agency (NEA–TDB) is the most comprehensive evaluation of thermodynamic data currently available for actinides, fission products and other elements relevant in the context of nuclear waste disposal. Technetium was initially reviewed in the volume 3 of the NEA–TDB series,[1] although the thermodynamic selection was later revisited in the update volume by Guillaumont and co-authors.[18] The outcome is a critically reviewed selection of Tc thermodynamic data, rather complete for Tc(VII)/Tc(IV) redox reactions and Tc(IV) solubility, hydrolysis and carbonate complexation as summarized in Table 1. $TcO_2{\cdot}xH_2O$(s) is the only Tc(IV) oxy-hydroxide solid phase selected in the NEA–TDB, and it is thus assumed to control the solubility of Tc(IV) over the complete pH-range except under very acidic conditions where Tc(IV)–Cl solid phases may form. The Tc(IV) hydrolysis scheme selected in the NEA–TDB includes the TcO^{2+} and $TcO(OH)^+$ species forming under acidic conditions, $TcO(OH)_2$(aq) prevailing within $3 \leq pH \leq 10$, and the anionic $TcO(OH)_3^-$ species dominating the aqueous chemistry of Tc(IV) under hyperalkaline pH conditions. The NEA–TDB performed this selection based only on the solubility studies by Meyer *et al.* (1991)[5] and Eriksen *et al.* (1992).[6]

Table 1 Stability constants currently selected in the NEA–TDB[18] for the solubility and hydrolysis of Tc(IV)

Solubility, $\log K_s^\circ$	
$TcO_2{\cdot}1.6H_2O(s) \Leftrightarrow TcO(OH)_2(aq) + 0.6H_2O(l)$	−8.4 ± 0.5
Hydrolysis, $\log \beta$	
$TcO(OH)_2(aq) + 2H^+ \Leftrightarrow TcO^{2+} + 2H_2O(l)$	<4
$TcO(OH)_2(aq) + H^+ \Leftrightarrow TcO(OH)^+ + H_2O(l)$	2.5 ± 0.8
$TcO(OH)_2(aq) + H_2O(l) \Leftrightarrow TcO(OH)_3^- + H^+$	−10.9 ± 0.4

The first definition of TcO^{2+} as Tc(IV) cation prevailing under very acidic conditions dates back to the electrophoretic study by Gorski and Koch (1969),[19] who reported a Tc(IV) species with charge +2 dominating at pH < 1.3. This formulation was adopted by the NEA–TDB, although more recent spectroscopic studies strongly hint towards the predominance of positively charged Tc(IV) polyatomic species under acidic conditions.[12–16] In spite of selecting the $TcO(OH)_3^-$ species, Rard and co-workers[1] acknowledged the need of additional experimental studies focussing on the alkaline pH region due to the limited number of data points in the study of Eriksen *et al.* (1992).[6] The lack of experimental studies at $I > 0.1$ M hindered the development of an activity model for Tc(IV), which remains as one of the main limitations of the current Tc(IV) thermodynamic selection in the NEA–TDB.

1.1.2 Activity models used in this work. The experimental conditions investigated in this study cover dilute ($I = 0.1$ M) to highly concentrated saline brine systems (up to $I = 13.5$ M). The use of this broad range of ionic strengths allows the assessment of Tc behaviour as a function of systematically varying chemical boundary conditions relevant for different disposal concepts (including disposal in rock-salt formations), but also permits an accurate extrapolation of the experimentally derived conditional equilibrium constants to $I = 0$ and simultaneous determination of the corresponding activity model. Both SIT and Pitzer activity models have been used in this study, SIT being the approach favoured by the NEA–TDB and Pitzer being the model widely recognized as the most accurate and most frequently used for extremely high ionic strengths (see the ESI†).

2 Materials and methods

2.1 Chemicals

All solutions were prepared with purified water (Milli-Q academic, Millipore) and purged for 2–3 hours with Ar before use. All sample preparation and handling procedures were performed in an Ar glovebox with <1 ppm O_2 at $T = 22 \pm 2$ °C.

A purified and radiochemically well-characterized ^{99}Tc stock solution (1.3 M $NaTcO_4$) was used for the electrochemical preparation of the Tc(IV) stock suspension. NaCl (p.a.), $MgCl_2{\cdot}6H_2O$ (p.a.), $Mg(OH)_2$(s), $CaCl_2{\cdot}2H_2O$ (p.a.), $Ca(OH)_2$(s), sodium dithionite ($Na_2S_2O_4$) and metallic iron powder (grain size 10 μm) were purchased from Merck. $SnCl_2$, pH buffers PIPES ($pK_a^\circ = 6.8$), TRIS ($pK_a^\circ = 8.3$) and tetraphenylphosphonium chloride (TPPC) were obtained from Sigma-Aldrich. HCl and NaOH Titrisol© (Merck) were used for adjusting the pH of the solutions.

2.2 pH and E_h measurements

The hydrogen ion concentration ($pH_m = -\log m_{H^+}$) was measured using combination pH electrodes (type ROSS, Orion) calibrated against standard pH buffers ($2 \leq pH \leq 12$, Merck). In salt solutions of ionic strength $I_m \geq 0.1$ mol kg^{-1}, the measured pH value (pH_{exp}) is an operational apparent value related to m_{H^+} by $pH_m = pH_{exp} + A_m$. The empirical correction factor A_m entails both the liquid junction potential and the activity coefficient of H^+. A_m values determined as a function of NaCl, $MgCl_2$ and $CaCl_2$ concentrations are available in the literature.[20,21] In NaCl–NaOH solutions with $m_{OH^-} > 0.03$ m, the H^+ concentration was calculated from the given m_{OH^-} and the conditional ion product of water.[18] In $MgCl_2$ and $CaCl_2$ solutions, the highest pH_m (pH_{max}) is fixed by the precipitation of $Mg(OH)_2$(s) and $Ca(OH)_2$(s) (or corresponding hydroxochlorides at Ca or Mg concentrations above ≈2 m), which buffer pH_m at ≈ 9 and ≈ 12, respectively.[20]

Redox potentials were measured with Pt combination electrodes with the Ag/AgCl reference system (Metrohm) and converted to E_h *vs.* the standard hydrogen electrode (SHE) by correction for the potential of the Ag/AgCl reference electrode (+208 mV for 3 M KCl at T = 22 °C). The measurement of E_h values in highly saline systems was previously discussed elsewhere.[11]

2.3 Sample preparation and characterization

The Tc(IV) solid phase used in this study was prepared by electrochemical reduction of a 0.01 M TcO_4^- solution in 1.0 M HCl at $E \approx -50$ mV *vs.* SHE, followed by quantitative precipitation of the Tc(IV) suspension in 5 mM $Na_2S_2O_4$ solution at $pH_m > 12$. The resulting $TcO_2{\cdot}xH_2O$(s) was aged for two months before further use.

The solubility of Tc(IV) was studied from undersaturation conditions in 0.1–5.0 M NaCl, 0.25–4.5 M $MgCl_2$ and 0.25–4.5 M $CaCl_2$ solutions. A total of 52 independent batch samples were prepared in these background electrolytes. The pH values were adjusted at $1.5 \leq pH_m \leq 14.5$ by using HCl–NaCl–NaOH, HCl–$MgCl_2$ and HCl–$CaCl_2$ of appropriate ionic strength, as well as $Mg(OH)_2$(s) and $Ca(OH)_2$(s). 0.5 M PIPES and 1.0 M TRIS stock solutions were used for buffering the solubility samples at $pH_m \approx 7$ and $pH_m \approx 8$, respectively. In both cases, the final buffer concentration was 12 mM. Based on a previous comprehensive study on the redox chemistry of Tc(VII)/Tc(IV) in dilute to concentrated saline systems,[11] $Na_2S_2O_4$, $SnCl_2$ and Fe powders (depending upon target pH) were used to stabilize the +IV redox state of Tc in the solubility samples. Background electrolyte solutions with adjusted pH_m and E_h conditions were equilibrated for two weeks. About 5 mg of the Tc(IV) solid phase were washed three times with 1 mL of the respective pre-equilibrated matrix solution and added to 20 mL of the same matrix solution in 50 mL screw cap centrifuge vials (Nalgene™, Thermo Scientific). Those samples with expectedly high solubility were prepared in smaller volumes (1 to 5 mL) to avoid the complete dissolution of the Tc(IV) solid phase. pH_m and m_{Tc} in the solubility samples were repeatedly measured at regular time intervals, usually from 3 to 600 days. During this time, samples were agitated manually about once per week. After reaching equilibrium conditions (stable pH_m and m_{Tc} readings), the pH of some unbuffered samples was slightly shifted by addition of acidic or basic solutions of the same ionic strength to obtain additional data points in the solubility curve. This approach was strictly followed from pH values with lower to higher solubility, in order to avoid oversaturation conditions and the potential formation of colloidal phases.[22]

Tc concentration in solution was quantified by Liquid Scintillation Counting (LSC, Quantulus, Perkin Elmer) after 10 kD ultrafiltration (2–3 nm, Pall Life Sciences). Samples for LSC analysis were mixed with 10 mL of LSC-cocktail Ultima Gold XR (Perkin-Elmer). The detection limit of LSC for this system was calculated as $\approx 4 \times 10^{-10}$ M (signal of the blank +3 standard deviations). The error associated with the sorption of Tc on the ultrafiltration filters was found below the uncertainty of the measurement of m_{Tc}. The oxidation state of Tc in the aqueous phase was determined by solvent extraction as reported elsewhere.[23,24] The supernatant of the sample was contacted with 50 mM TPPC in chloroform. After vigorous mixing for 1 minute and subsequent separation of the aqueous and organic phases by centrifugation, Tc concentration in the aqueous phase was determined by LSC. Since TcO_4^- is extracted to the organic solvent, the activity remaining in the aqueous phase is interpreted as Tc(IV).

Solid phase characterization was conducted for selected batch samples after attaining equilibrium conditions. A fraction of the solid phase (≈ 1 mg) was washed 3–5 times with ethanol under an Ar atmosphere to remove the salt-containing matrix solution. After the last cleaning step, the solid was resuspended in approximately 20 μL ethanol, transferred to a capped silicon single crystal sample holder (Dome, Bruker), dried under an Ar atmosphere for a few minutes before sealing of the sample holder, and transferred outside the glovebox for the collection the XRD diffractogram. XRD measurements were performed on a Bruker AXS D8 Advance X-ray powder diffractometer at $10° \leq 2\theta \leq 78°$ with incremental steps of 0.015° and a measurement time of 1.7 seconds per step. The spectra collected were compared with the JCPDS database (Joint Committee on Powder Diffraction Standards[25]). After XRD measurement, the solid phase was dissolved in 1 mL of 2–3% HNO_3 and used for quantitative chemical analysis. The dissolved solid phase was analysed by LSC and inductively coupled plasma-optical emission spectroscopy (ICP-OES,

Perkin-Elmer Optima 2000™) to determine the Tc and Na, Mg, or Ca contents, respectively. Analytical errors in the quantitative chemical analysis by LSC and ICP–OES can be safely considered to be below 10%. A second fraction of the washed solid was investigated in the selected samples by scanning electron microscope-energy disperse spectrometry (SEM–EDS) with the aim of characterizing the morphology and crystallinity of the solid phase, and to further assess its chemical composition. Measurements were performed with a FEI Quanta 650 FEG equipped with a Noran EDS unit.

The number of hydration waters in the $TcO_2{\cdot}xH_2O$(s) solid phase used in the present work before and after solubility experiments was quantified by thermogravimetric analysis (TG–DTA) using a Netzsch STA 449C equipment. Three samples were prepared for thermogravimetric analysis: (i) 6.6 mg of the original Tc(IV) solid phase prepared by electrolysis and consecutive precipitation in alkaline media (presence of $Na_2S_2O_4$, $pH_m \approx 12$), (ii) 6.1 mg of the Tc(IV) solid phase equilibrated in 5.0 M NaCl (presence of $Na_2S_2O_4$, $pH_m = 12$, 13 and 14) and (iii) 1.4 mg of the Tc(IV) solid phase equilibrated in 4.5 M $MgCl_2$ (presence of Sn(II), $pH_m = 4$). All investigated samples were washed 3–5 times with ethanol under an Ar atmosphere to remove the salt-containing matrix solution. After the last cleaning step, the solid was left to dry under an Ar atmosphere for 2–3 days and transferred to a glovebox specifically dedicated to DTA analyses. Measurements were performed under an Ar atmosphere up to $T = 200$ °C at a rate of 5 K min^{-1}.

2.4 XAFS measurements

XAFS spectra were recorded at the INE-Beamline for Actinide Research at ANKA, KIT Campus North,[26] in Karlsruhe, Germany. Both solid and aqueous phases were characterized by XANES/EXAFS to confirm the redox state of Tc and assess its coordination environment. Three samples were investigated: (i) the original Tc(IV) solid phase, (ii) a Tc(IV) solid phase equilibrated in 4.5 M $CaCl_2$ at $pH_m = 11.4$ and (iii) the supernatant solution of the solubility sample equilibrated in 4.5 M $MgCl_2$ at $pH_m = 2.0$ ($m_{Tc} \approx 3 \times 10^{-3}$ m). In all cases, approximately 300 μL of the suspension were transferred to a 400 μL polyethylene vial under an Ar atmosphere and centrifuged at 4020*g* for 10 minutes to obtain a compacted solid phase at the bottom of the vial. The vials were mounted in a gas-tight cell with windows of the Kapton® film (polyimide) inside the Ar-glovebox and transported to the INE-Beamline. XAFS measurements were conducted within a few hours after sample preparation.

Tc-K edge (21 044 eV) XAFS spectra (3–4 replicates per sample) were recorded at room temperature under a continuous flow of Ar. Ge(422) crystals were used in the double crystal monochromator, Lemonnier-type operating in fixed-exit mode. The monochromatic beam is focused by a toroidal mirror, delivering a beam spot-size of ~500 × 300 μm^2 at the sample position at a photon energy of 18 keV. The parallel alignment of the crystal faces was detuned to ≈70% of the maximum beam intensity at the beginning of each scan. The incident intensity was held constant by means of a piezo-driven feedback system to the second crystal. The intensity of the incoming beam (I0) was monitored using an Ar filled ionization chamber at ambient pressure. Spectra were recorded in fluorescence mode using a five pixel LEGe solid state detector (Canberra, Belgium). Tc spectra were energy-calibrated with respect to the first inflection point in the XANES spectra of a Mo metal foil (20 000 eV), which was measured simultaneously in transmission geometry.

XANES/EXAFS data reduction and analysis were performed with the ATHENA/ARTEMIS package following standard procedures.[27] Structural information was obtained following a multi-shell step-wise approach for the EXAFS data fitting. The fit included the neighbouring atomic distances (R), EXAFS Debye–Waller factors (σ^2), coordination numbers (CN) and relative shift in ionization energy E_0 (ΔE_0). EXAFS spectra were Fourier transformed (FT) in the k-range between 2.6–10.4 $Å^{-1}$ and 2.0–8.5 $Å^{-1}$ using Hanning windows for solid and aqueous phases, respectively. The fit was performed in R-space (1.2–2.5 Å) using paths files calculated with Feff8.4 based on the TcO_2 crystal structure reported in the ICSD database with record number 17–3151. The coordination number of O-shells was allowed to vary in the fit, whereas Tc- and Cl-shells were constrained to 1 and 1.4, respectively. The value of 1.4 for Cl in the fit of aqueous phases was obtained in a preliminary fit where CN(Cl) was defined such that the total CN(O) + CN(Cl) for the first coordination shell was equal to 6. The overall amplitude factor S_0^2 was set to 0.75 to obtain a good match with the coordination number of ~6 in the solid and reference samples.

2.5 Quantum chemical calculations

The stability of the complexes $[TcO(OH)_5]^{3-}$ and $Ca_n[TcO(OH)_5]^{2n-3}$ (n = 1–3) in gas and aqueous phases was investigated by quantum chemical calculations using a combination of multi reference *ab initio* methods and density functional theory (DFT). Only multi reference *ab initio* calculations on TcO (ref. 28) and density functional theory (DFT) calculations on TcO^{2+} (ref. 29) have been previously reported in the literature, whereas no accurate high-level multireference *ab initio* calculations on TcO^{2+} are available to date. Provided that TcO^{2+} is at the core of these complexes, the lack of these calculations prevents a theoretically sound characterization of the lowest electronic state. Consequently, we performed pilot studies on TcO^{2+} with high-level multireference Complete Active Space Self Consistent Field (CASSCF) and Multi Reference Configuration Interaction (MRCI) calculations to identify the electronic configuration of the ground states of these species.[30] This is a very important pre-requisite for the theoretically sound application of DFT, which is restricted to single reference states. Calculations were first performed in the gas phase, and then extended to a simulated aqueous system consisting of a water cluster with 100 water molecules. This cluster was previously described by Müller *et al.* and Lenz and Ojamäa.[31–33]

3 Results and discussion

3.1 Solubility of Tc(IV) in dilute to concentrated NaCl solutions

Fig. 1 shows the experimental solubility data obtained in the present work in dilute to concentrated NaCl systems, compared with solubility data previously reported in the literature (Meyer *et al.*, 1991;[5] Eriksen *et al.*, 1992;[6] Hess *et al.*, 2004;[7] Warwick *et al.*, 2007[9]). In the acidic pH region, experimental data in 0.1 M NaCl agree well with the previous solubility data in dilute systems reported by Meyer *et al.* (1991).[5] The solubility of Tc(IV) within $2.5 \leq pH_m \leq 4$ increases up to 3 orders of magnitude with increasing ionic strength. This trend qualitatively agrees with previous experiments reported by Hess *et al.* (2004)[7] (see also Fig. 1). Strong kinetics are observed for the sample at $pH_m \approx 2$ in 5.0 M NaCl, for which equilibrium is not attained even after 520 days of contact time. Note that slow kinetics were also observed by Hess and co-workers in their solubility experiments, in spite of considering significantly shorter equilibration times (≤61 days).

All investigated NaCl systems follow a well-defined slope of −2 ($\log m_{Tc(IV)}$ *vs.* pH_m, dashed lines in Fig. 1) within the pH_m-range 1.5 to 4, which indicates that 2 H^+ are consumed in the chemical reaction controlling the solubility of Tc(IV) in this pH region. This observation agrees very well with the slope analysis in the study of Meyer *et al.*,[5] whereas it is in disagreement with the slope of −1 proposed by Hess *et al.*[7] Note that Hess and co-workers disregarded their solubility data at longer equilibration times for the slope analysis (and thus for the definition of their chemical model), which was mostly based on solubility data gained after 11 days of equilibration time. Provided the strong kinetics observed (both in the present work and in Hess *et al.*) for the solubility equilibria under acidic conditions, we consider that the interpretation by the latter authors is not representing the thermodynamic equilibrium under these conditions (see Fig. A1 in the ESI†).

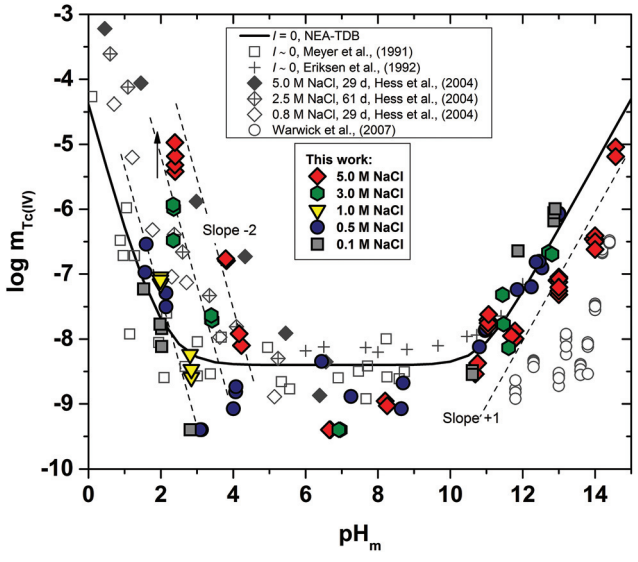

Fig. 1 Tc(IV) experimental solubility data determined in this work in dilute to concentrated NaCl solutions. Solubility data reported in the literature under analogous experimental conditions appended in the figure for comparison purposes. Solid line corresponds to the overall solubility curve of $TcO_2 \cdot 1.6H_2O$(s) calculated at I = 0 with the current NEA–TDB thermodynamic selection for Tc(IV). Dashed lines indicate the slope analysis performed in the present work. The arrow shows the time dependency of the indicated sample.

At $4 \leq pH_m \leq 9$, a pH-independent solubility behaviour is observed in dilute to concentrated NaCl solutions, indicating that no H^+ are exchanged in the chemical reaction controlling the solubility of Tc(IV) in this pH-region. The concentration of Tc is not affected by ionic strength either, and thus data in 0.1 M and 5.0 M NaCl show similar solubility. A very large scattering in m_{Tc} (1–1.5 log-units) is observed in this pH region. This behaviour is likely related with the very low solubility (close to the detection limit of LSC) and the expected predominance of neutral species in solution, which are prone to form oligomeric species and strongly sorb on surfaces (filters, vessel walls, solid phases, *etc.*). A similar behaviour was previously reported for An(III)/Ln(III) and An(IV).[22,34] Meyer and co-workers reported very similar observations, *i.e.* pH- and ionic strength independent behaviour and large scattering of the solubility data. Although not discussed in the original publication, we hypothesize that the very stable Tc concentrations measured by Eriksen *et al.* (1992)[6] within $6 \leq pH \leq 10$ ($\log m_{Tc} = -8.2$) likely correspond to the detection limit of their quantification method.

The solubility of Tc(IV) increases with a well-defined slope of +1 ($\log m_{Tc(IV)}$ *vs.* pH_m) at $pH_m \geq 11$. Although the same slope is retained, the solubility decreases almost one order of magnitude when increasing the ionic strength from 0.1 to 5.0 M NaCl. Note that a similar trend with increasing ionic strength was reported for the solubility of Zr(IV) under alkaline to hyperalkaline pH conditions,[21] where anionic hydrolysis species are dominant in solution. The solubility data and slope determined in this work in 0.1 M NaCl are consistent with the results reported by Eriksen *et al.* (1992).[6] Significantly lower Tc(IV) solubility was observed by Warwick *et al.* (2007)[9] within $12 \leq pH \leq 14$. Unfortunately, the authors did not properly characterize the solid phase controlling the solubility. Although a solubility-control by a more crystalline Tc(IV) solid phase can be hypothesized, a direct comparison with the solubility data gained in this work is not feasible.

3.2 Solubility data of Tc(IV) in dilute to concentrated $MgCl_2$ solutions

Fig. 2 shows the experimental solubility data obtained in the present work in dilute to concentrated $MgCl_2$ systems. The solubility of Tc(IV) in the acidic pH region is nearly identical to the solubility data obtained in NaCl solutions with similar ionic strength, indicating that the same chemical reaction likely controls the solubility in both systems. Within the same pH-region, the solubility of Tc(IV) is significantly increased (up to 5 orders of magnitude) with the increasing $MgCl_2$ concentration. This observation reflects very strong ion interaction processes taking place between cationic Tc(IV) hydrolysis

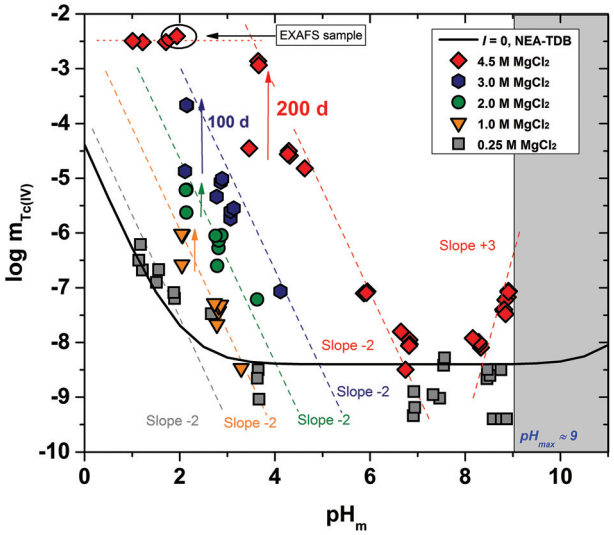

Fig. 2 Tc(IV) experimental solubility data determined in this work in dilute to concentrated $MgCl_2$ solutions with $2 \leq pH_m \leq 9$. Solid line corresponds to the overall solubility curve of $TcO_2{\cdot}1.6H_2O$(s) calculated at $I = 0$ with the current NEA–TDB thermodynamic selection for Tc(IV). Dashed lines indicate the slope analysis performed in the present work. Shadowed area designates the precipitation of $Mg(OH)_2$(s) ($[MgCl_2] \leq 2$ M) or Mg–OH–Cl(s) ($[MgCl_2] \geq 2$ M). Arrows show the time dependency of the indicated samples.

species and Cl^-, although the possible formation of new aqueous species must also be considered. The solubility curve becomes pH-independent in 4.5 M $MgCl_2$ solutions with $pH_m \leq 2$ (dotted lines in Fig. 2). A similar behaviour was reported by Hess *et al.* (2004)[7] at $pH_m \leq 0.1$ and $pH_m \leq 0.75$ in pure HCl and 5.0 M HCl–NaCl systems, respectively. Hess and co-workers explained this observation considering a solid phase transformation from $TcO_2{\cdot}xH_2O$(s) to $TcCl_4$(s) and assuming the predominance of $TcCl_4$(aq) in the aqueous phase. In the present work, the aqueous speciation of Tc in 4.5 M $MgCl_2$ solutions with $pH_m \leq 2$ has been investigated by XAFS and is discussed in section 3.4.3. Slow kinetics are observed in solubility samples in contact with $[MgCl_2] \geq 2$ M, where equilibrium conditions (stable pH_m and m_{Tc} readings) are only attained after 200 days. Considering m_{Tc} data collected at longer equilibration times, the solubility curves of all evaluated $MgCl_2$ systems follow a very well-defined slope of −2 within the pH_m-range 2 to 6 (depending upon salt concentration). This is in excellent agreement with the solubility data obtained in the present work in NaCl systems and indicates that $2H^+$ are consumed in the chemical reaction controlling the solubility in this pH region.

The solubility of Tc(IV) shows a pH-independent behaviour at $4 \leq pH_m \leq 9$ in 0.25 M $MgCl_2$, in analogy with the NaCl systems. The pH-independent region is significantly smaller in 4.5 M $MgCl_2$ ($7 \leq pH_m \leq 8$), mainly due to the very relevant increase in the solubility under acidic pH conditions, but also because of a likely change in the aqueous speciation above $pH_m \approx 8$. As in the case of NaCl systems, the solubility of Tc(IV) in this pH region scatters within $-8.2 \geq \log m_{Tc} \geq -9.4$.

A steep increase in the Tc(IV) solubility is observed in 4.5 M $MgCl_2$ solutions with $pH_m \approx 8$. This behaviour differs from the findings gained in the NaCl systems, where the formation of anionic Tc(IV) hydrolysis species (and consequent increase of the solubility) takes only place at $pH_m \approx 11$. Similar observations were previously reported for Zr(IV) and An(IV) in concentrated alkaline $CaCl_2$ solutions.[21,35,36] Based on the collected spectroscopic evidence (EXAFS) and model calculations, the solubility behaviour of Zr(IV) and An(IV) under these conditions was explained with the formation of ternary Ca–Zr(IV)/An(IV)–OH aqueous species. The predominance of analogous Mg–Tc(IV)–OH aqueous species is accordingly suspected in concentrated alkaline $MgCl_2$ solutions, in spite of the limitations in pH_m posed by the precipitation of Mg–OH–Cl(s) ($pH_{max} \approx 9$). In order to gain more conclusive insights into the aqueous chemistry of Tc(IV) in concentrated alkaline MCl_2 ($M = Mg^{2+}$, Ca^{2+}) systems, the solubility of Tc(IV) was further investigated in dilute to concentrated alkaline $CaCl_2$ solutions and is discussed in the following section.

3.3 Solubility data of Tc(IV) in dilute to concentrated $CaCl_2$ solutions

The experimental solubility data obtained in $CaCl_2$ solutions within $7 \leq pH_m \leq 12$ are shown in Fig. 3. The solubility of Tc(IV) in 0.25 M $CaCl_2$ follows a pH-independent behaviour up to $pH_m \approx 11$. A very steep but slow increase in solubility is observed in more concentrated $CaCl_2$ systems. Hence, the solubility of Tc(IV) in 4.5 M $CaCl_2$ increases 3 orders of magnitude within $9.5 \leq pH_m \leq 10.5$ following a well-defined slope of

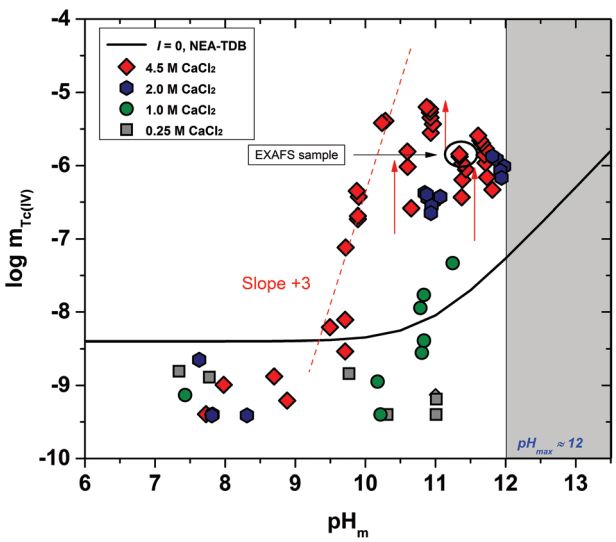

Fig. 3 Tc(IV) experimental solubility data determined in this work in dilute to concentrated $CaCl_2$ solutions with $7 \leq pH_m \leq 12$. Solid line corresponds to the overall solubility curve of $TcO_2{\cdot}1.6H_2O$(s) calculated with the NEA–TDB for $I = 0$. Dashed lines indicate the slope analysis performed in the present work. Shadowed area designates the precipitation of $Ca(OH)_2$(s) ($[CaCl_2] \leq 2$ M) or Ca–OH–Cl(s) ($[CaCl_2] \geq 2$ M) solid phases. Arrows show the time dependency of the indicated samples.

+3 ($\log m_{Tc(IV)}$ *vs.* pH_m, dashed line in Fig. 3). For this system, equilibrium conditions are not attained above $pH_m \approx 10.5$ even after 325 days. The very steep increase in solubility cannot be explained with the formation of $TcO(OH)_3^-$ as described for NaCl systems, but rather points to the predominance of higher hydrolysis species strongly interacting with Ca^{2+} ions. In this context, the possible formation of ternary Ca–Tc(IV)–OH aqueous complexes is discussed in section 4 in combination with the outcome of DFT calculations summarized in section 3.4.4. The possible formation of ternary Ca–Tc(IV)–OH solid phases in concentrated hyperalkaline $CaCl_2$ systems was assessed by EXAFS and is discussed in section 3.4.3.

3.4 Tc aqueous and solid phase characterization

3.4.1 Tc redox speciation (solvent extraction). Solvent extraction was performed with the supernatant solution (after 10 kDa ultrafiltration) of selected solubility samples with $m_{Tc} \geq 10^{-6.5}$ m. Table 2 shows the results of the redox distribution of Tc in NaCl and $MgCl_2$ solutions. In NaCl solutions, solvent extraction confirms the predominance of Tc(IV) in the aqueous phase. This observation is consistent with the predictions based on the measured pH_m and E_h values and the Tc *Pourbaix* diagrams reported by Yalcintas *et al.* (2015).[11] In 4.5 M $MgCl_2$ solutions with pH_m = 2 and 4, solvent extraction suggests that only 13% and 52% of total m_{Tc} corresponds to Tc (IV), respectively. The fraction of Tc(IV) becomes predominant (90–95%) at $pH_m \approx 9$. Similar Tc(VII)/Tc(IV) redox distributions were obtained in our previous study in 4.5 M $MgCl_2$ systems.[11] The redox state of Tc in the aqueous phase and the potential impact of Tc(IV)–Cl complex formation to the solvent extraction method are discussed in detail in section 3.4.3, in connection with XANES/EXAFS measurements.

3.4.2 Solid phase characterization: XRD, SEM–EDS, quantitative chemical analysis and TG–DTA. Table 3 shows the results of the solid phase characterization by XRD and quantitative chemical analysis, accomplished for selected solubility samples in NaCl, $MgCl_2$ and $CaCl_2$ systems. XRD characterization of Tc solid phases equilibrated in NaCl and $MgCl_2$ solutions shows broad patterns, reflecting the amorphous character of the solid phases controlling the solubility in these systems (Fig. 4, left). Note that Tc(IV) oxide normally exists as a hydrous amorphous solid phase ($TcO_2{\cdot}xH_2O$(s)), which provides no marked reflections in powder XRD. The crystalline TcO_2(cr) has been reported to form by thermal decomposition of NH_4TcO_4,[37,38] and it is not expected under the experimental conditions used in this work. XRD patterns collected for solid phases equilibrated in 4.5 M $CaCl_2$ with Sn(II) as the reducing agent systematically show the presence of unknown peaks at 2Θ = 11.6, 23 and 33 (Fig. 4, right). These features could not be assigned to any compound currently selected in the JCPDS database for Tc, Ca and/or Sn.[25] In the absence of these peaks in 4.5 M $CaCl_2$ solutions of analogous pH_m but with $Na_2S_2O_4$ as the reducing agent, the features under discussion are attributed to the formation of a Ca–Sn–OH solid phase.

The SEM images (Fig. 5 and 6) of all investigated samples show the predominance of amorphous Tc aggregates, in good agreement with the observed absence of well-defined XRD patterns. The particle size of these aggregates varies between 50 and 80 nm. Quantitative chemical analyses (Table 3) show the absence of Na in the Tc solid phases controlling the solubility in NaCl systems, even for those phases equilibrated in 5.0 M NaCl solutions. Similarly, no Mg is detected in solid phases controlling the solubility under acidic conditions in 4.5 M $MgCl_2$, whereas very high Mg content is quantified in alkaline samples with $pH_m \approx pH_{max}$. SEM images of the later samples confirm the presence of needle-like precipitates of Mg–OH–Cl (s) (Fig. 5, right). Similar observations are gained for Tc solid phases equilibrated in $CaCl_2$ solutions with $pH_m \approx pH_{max}$, for which SEM pictures indicate the presence of $Ca(OH)_2$(s) and/or

Table 2 Fraction of Tc(IV) in the aqueous phase of selected solubility samples as quantified by solvent extraction after 10 kD ultrafiltration. Reducing chemicals and measured pH_m and E_h for each sample are also provided

Background electrolyte	Reducing system	pH_m [a]	E_h [b] (mV)	%Tc(IV)[c]
0.5 M NaCl	$Na_2S_2O_4$	12.4	−670	99
5.0 M NaCl	Sn(II)	2.5	80	99
5.0 M NaCl	$Na_2S_2O_4$	13.0	−540	98
5.0 M NaCl	$Na_2S_2O_4$	14.0	−580	98
4.5 M $MgCl_2$	Sn(II)	2.0	n.m.	13[d]
4.5 M $MgCl_2$	Sn(II)	4.0	−50	52
4.5 M $MgCl_2$	Fe Powder	8.9	−170	91
4.5 M $MgCl_2$	Sn(II)	9.0	−175	94

[a] ± 0.05. [b] ± 50 mV. [c] ± 10%; n.m. = not measured. [d] Same sample also investigated by XAFS.

Table 3 Summary of XRD and quantitative chemical analysis conducted for selected Tc solid phases equilibrated in NaCl, $MgCl_2$ and $CaCl_2$ systems

Background electrolyte	Reducing system	pH_m [a]	XRD	Chemical analysis Na : Tc
0.5 M NaCl	$Na_2S_2O_4$	12.4	am	<0.01
5.0 M NaCl	Sn(II)	2.5	am	<0.01
5.0 M NaCl	$Na_2S_2O_4$	13.0	n.m.	<0.01
5.0 M NaCl	$Na_2S_2O_4$	14.0	am	<0.01
				Mg : Tc
0.25 M $MgCl_2$	Sn(II)	2.0	am	<0.01
4.5 M $MgCl_2$	Sn(II)	4.0	am	<0.01
4.5 M $MgCl_2$	Fe Powder	8.9	n.m.	25.0[b]
4.5 M $MgCl_2$	Sn(II)	9.0	n.m.	0.3[b]
				Ca : Tc
2.0 M $CaCl_2$	$Na_2S_2O_4$	11.8	am	n.m.
4.5 M $CaCl_2$	Sn(II)	10.9	am, (11.6, 23, 33)	2.7[c]
4.5 M $CaCl_2$	$Na_2S_2O_4$	11.7	am	1.6[c]
4.5 M $CaCl_2$	Sn(II)	11.4	am, (11.6, 23, 33)	n.m.
4.5 M $CaCl_2$	Sn(II)	10.7	am, (11.6, 23, 33)	n.m.

[a] ± 0.05, n.m. = not measured. [b] pH = pH_{max}, presence of Mg–OH–Cl(s) expected. [c] pH = pH_{max}, presence of Ca–OH–Cl(s) expected.

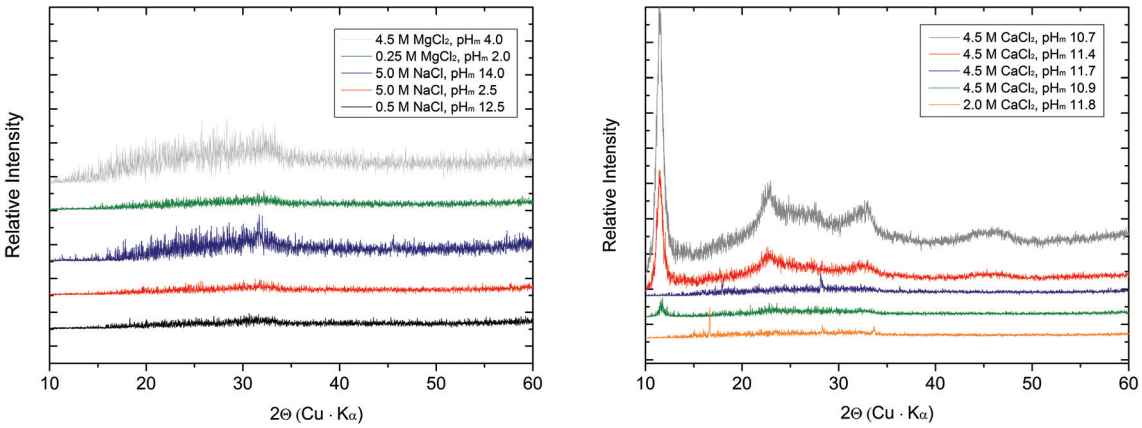

Fig. 4 XRD patterns collected for Tc solid phases equilibrated in dilute to concentrated NaCl and $MgCl_2$ solutions (left), and concentrated $CaCl_2$ solutions (right).

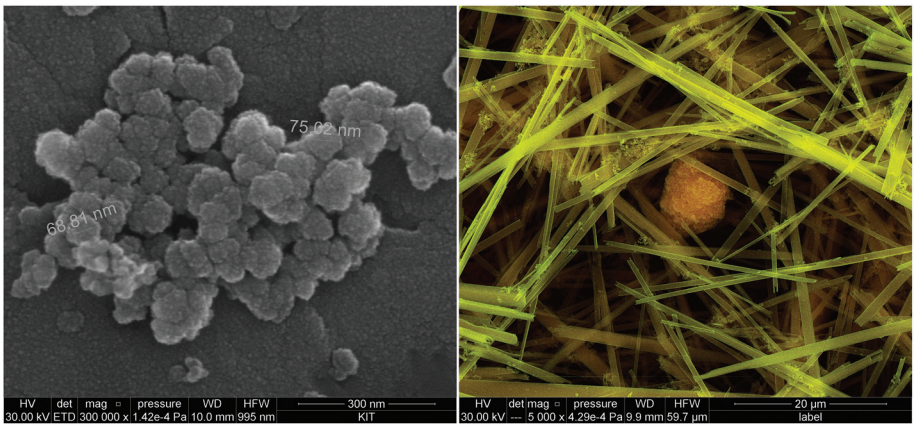

Fig. 5 SEM pictures of Tc solubility samples equilibrated in 0.5 M NaCl at pH_m = 12.4 (left) and in 4.5 M $MgCl_2$ at pH_m = 9.0 (right). In the right sample, the coexistence of amorphous $TcO_2{\cdot}xH_2O$(s) aggregates and needle like Mg-oxyhydroxide phases is observed.

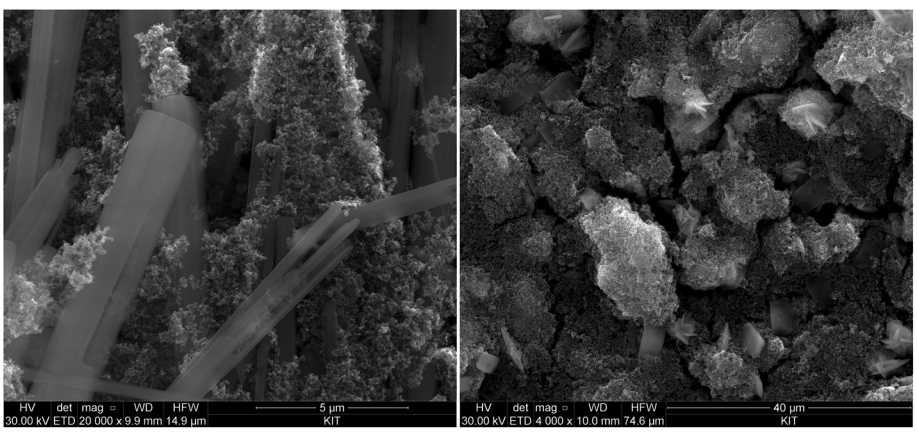

Fig. 6 SEM pictures of Tc solubility samples equilibrated in 4.5 M $CaCl_2$ at pH_m = 10.7 (left) and in 2.0 M $CaCl_2$ at pH_m = 11.8 (right). Coexistence of Ca-oxyhydroxide and Ca-S phases is observed in the left and right samples, respectively.

Ca–OH–Cl(s) phases (Fig. 6). The absence of Na, Mg, or Ca in the Tc solid phases (except those at $pH_m \approx pH_{max}$) controlling the solubility in NaCl, $MgCl_2$ and $CaCl_2$ systems, in combination with the amorphous character of the solid confirmed by XRD and SEM, strongly points towards a solubility-control exerted by $TcO_2{\cdot}xH_2O$(s).

TG–DTA analyses indicate a mass loss of 5–11% in the investigated solid phases, corresponding to x = 0.4–0.8 in $TcO_2{\cdot}xH_2O$(s). These results highlight the similar hydration degree of the Tc(IV) solid phase in the different background electrolytes and salt concentrations considered in this study. The unweighted mean value of the number of hydration waters $x = 0.6 \pm 0.3$ is considered in the following in the definition of the Tc(IV) solid phase used in this study: $TcO_2{\cdot}0.6H_2O$(s). Note that a very discrepant number of hydration waters was previously reported by Meyer and co-workers,[5] who measured x = 0.44–4.22 and 1.38–1.81 for solid phases obtained from acidic and alkaline deposition, respectively. Although the number of hydration waters has a minor influence on solubility phenomena and calculations in dilute systems, it becomes relevant in concentrated brines where water activities significantly lower than 1 arise (*e.g.* a_w = 0.5083 in 4.0 M $MgCl_2$).[18]

3.4.3 XANES/EXAFS. Fig. 7 shows the Tc K-edge XANES spectra of the three investigated samples, namely the original $TcO_2{\cdot}0.6H_2O$(s) material, the Tc(IV) solid phase equilibrated in 4.5 M $CaCl_2$ at pH_m = 11.4 (see also Fig. 3) and the supernatant of the Tc(IV) solubility sample equilibrated in 4.5 M $MgCl_2$ at pH_m = 2 (see also Fig. 2). The figure also shows Tc(IV)(s) and Tc(VII)(aq) XANES reference spectra collected at the INE-Beamline. The shape and energy position of the inflection point in the XANES spectra unequivocally confirm the only presence of Tc(IV) (within the detection limit of the technique, ~5–10%) in all investigated samples. Note that the results obtained by solvent extraction, *i.e.* a very low fraction of Tc(IV) in the supernatant of the solubility sample equilibrated in 4.5 M $MgCl_2$ at pH_m = 2 (13%, see Table 2) are not confirmed by XANES showing Tc(IV) only.

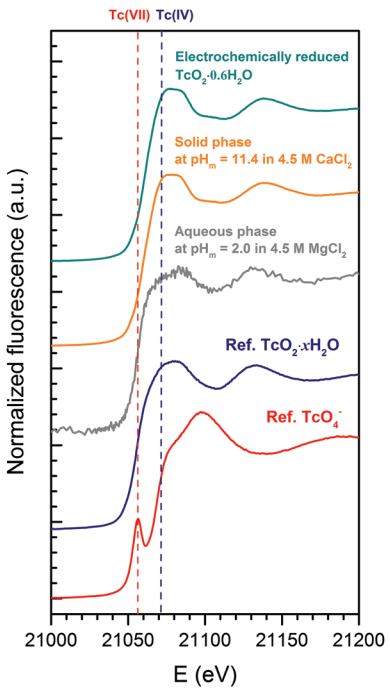

Fig. 7 Tc K-edge XANES spectra of the original $TcO_2{\cdot}0.6H_2O$(s) material (green), Tc(IV) solid phase equilibrated in 4.5 M $CaCl_2$ at pH_m = 11.4 (orange) and the supernatant solution in the solubility sample equilibrated in 4.5 M $MgCl_2$ at pH_m = 2 (gray). Reference spectra for Tc(IV) ($TcO_2{\cdot}xH_2O$(s), blue) and Tc(VII) (TcO_4^-, red) collected at the INE-Beamline are appended in the figure for comparison.

k^2-weighted Tc K-edge EXAFS spectra and corresponding Fourier transforms are shown in Fig. 8. Structural parameters of all investigated samples resulting from the fit of the EXAFS spectra are summarized in Table 4. The EXAFS fit of the original $TcO_2{\cdot}0.6H_2O$(s) material shows an O-shell at 2.07 Å with a coordination number (CN) of 6.7, and a Tc-shell at 2.59 Å with CN = 1. These results are in excellent agreement with structural parameters reported in the literature for $TcO_2{\cdot}xH_2O$(s).[7] Similar structural parameters are obtained from the fit to EXAFS data of the Tc(IV) solid phase equilibrated in 4.5 M $CaCl_2$ at pH_m = 11.4. This observation indicates that no solid phase transformation occurred within the 325 days of equilibration time, and that $TcO_2{\cdot}0.6H_2O$(s) remains as the solubility-controlling phase under these conditions. Hence, Tc(IV) solubility data obtained in $[CaCl_2] \geq 2.0$ M at $pH_m \approx pH_{max}$ are not representative of a thermodynamic equilibrium and can only be explained by the very slow kinetics in the presence of $Ca(OH)_2$(s) or Ca–OH–Cl(s) phases or eventually a solubility control by an unidentified surface "coating".

The EXAFS fit of the supernatant solution in the solubility sample equilibrated in 4.5 M $MgCl_2$ at pH_m = 2 unequivocally shows the co-existence of O- (CN = 3.5, R = 2.21 Å) and Cl- (CN = 1.4, R = 2.53 Å) backscatterers in the first coordination sphere of Tc. The substitution of Tc–Cl by Tc–O interactions significantly worsens the fit. The addition of a Tc–Tc contribution at R = 2.77 Å decreased the residual of the fit (%R), although this farther shell was disregarded in the final model due to the limited k-range considered in the fit ($2.0 \leq k\,[Å^{-1}] \leq 8.5$). These observations hint towards the possible formation of Tc(IV)–O/OH–Cl oligomers in acidic concentrated $MgCl_2$ solutions. Note that Poineau and co-workers[16] reported the predominance of the $Tc_2OCl_{10}^{4-}$ species at pH = 0.3 and $[Cl^-]$ = 3.0 M. The structural parameters determined for this species by EXAFS for Tc–O (CN = 1.2, R = 1.79 Å) and Tc–Cl (CN = 4.7, R = 2.36 Å) interactions are significantly different compared to those determined in the present study, suggesting the predominance of a different aqueous species at pH_m = 2.0 and $[Cl^-]$ = 9.0 M (present work). The formation of Tc(IV) – chloride species in acidic concentrated $MgCl_2$ solutions is in line with the results obtained by liquid–liquid extraction. Hence, the solvent extraction method used in the present work has been reported to extract into the organic phase not only MO_4^- species, but also anionic chloride complexes.[39]

3.4.4 Quantum mechanical calculations: density Functional theory (DFT). Multireference CASSCF and MRCI calcu-

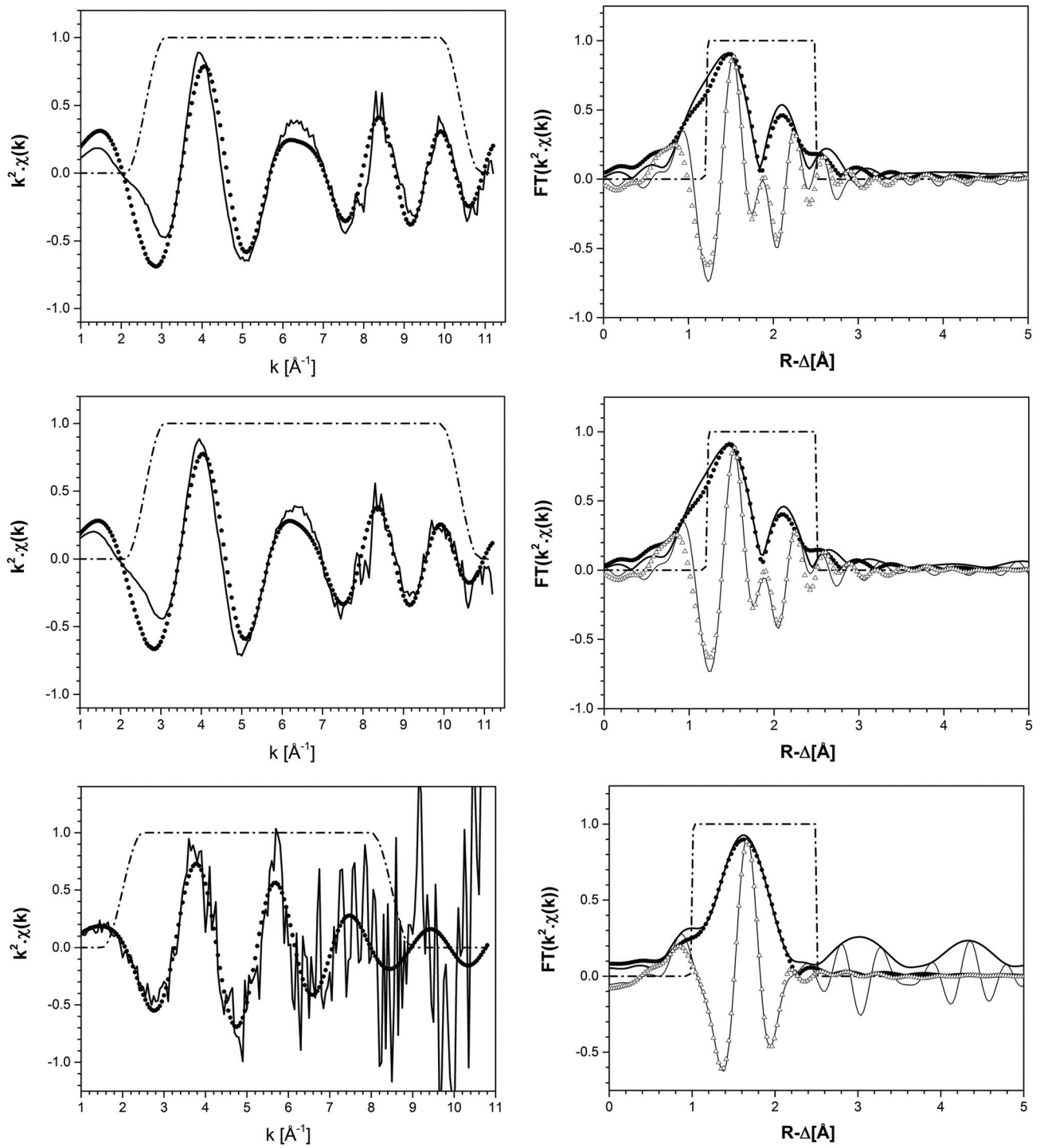

Fig. 8 k^2-Weighted EXAFS spectra and Fourier Transform of the original $TcO_2{\cdot}0.6H_2O$(s) material (top), Tc(IV) solid phase equilibrated in 4.5 M $CaCl_2$ at pH_m = 11.4 (middle), and the supernatant solution in the solubility sample equilibrated in 4.5 M $MgCl_2$ at pH_m = 2 (bottom). Experimental data are depicted as solid lines, whereas fits are shown as circles and triangles (modulus and imaginary parts, respectively). Dashed lines correspond to the FT hanging windows used in the EXAFS fit.

lations show that the lowest doublet and quartet states of TcO^{2+} are single reference states. Hence, the ground states of the hydrolysis species $TcO(OH)_y^{2-y}$ are also quartet single reference states and therefore the application of large-scale DFT calculations is permitted. This allows for investigating the stoichiometry and structure of relevant Tc(IV) species forming in alkaline $CaCl_2$ solutions, which otherwise cannot be assessed spectroscopically due to the low Tc(IV) concentrations in solution.

Table 4 Structural parameters obtained from the EXAFS evaluation of the original $TcO_2{\cdot}0.6H_2O$(s) material, Tc(IV) solid phase equilibrated in 4.5 M $CaCl_2$ at pH_m = 11.4, and the supernatant solution in the solubility sample equilibrated in 4.5 M $MgCl_2$ at pH_m = 2

Sample	Path	CN	R (Å)	σ^2 (Å^2)	ΔE_0 (eV)	R-factor
Original $TcO_2{\cdot}0.6H_2O$(s) material	Tc–O	6.7	2.07	0.010	−5.146	0.002
R-Space [1.2–2.5 Å]	Tc–Tc	1.0[a]	2.59	0.002		
k-Range [2.6–10.4 Å^{-1}]						
Tc(IV) solid phase in 4.5 M $CaCl_2$ at pH_m = 11.4	Tc–O	6.4	2.07	0.009	−5.635	0.015
R-Space [1.2–2.5 Å]	Tc–Tc	1.0[a]	2.59	0.003		
k-Range [2.6–10.4 Å^{-1}]						
Tc(IV)(aq) in 4.5 M $MgCl_2$ at pH_m = 2	Tc–O	3.5	2.21	0.002	0.842	0.010
R-Space [1.0–2.5 Å]	Tc–Cl	1.4[a]	2.53	0.007		
k-Range [2.0–8.5 Å^{-1}]						

Fit errors: CN: ± 20%, R: 0.01 Å, σ^2: 0.001 Å^2. [a] Held constant during the fit.

Tc(IV) solubility data obtained in concentrated $CaCl_2$ solutions hint towards the formation of the previously unreported $[TcO(OH)_5]^{3-}$ moiety in the aqueous phase, considering the slope of +3 ($\log m_{Tc}$ *vs.* pH_m) and the solubility control by $TcO_2{\cdot}0.6H_2O$(s). In the absence of Ca in the background electrolyte (*e.g.* NaCl or KCl systems), $TcO(OH)_3^-$ is the only anionic hydrolysis species forming under hyperalkaline pH conditions (see section 3.1 and references therein). As previously described for Zr(IV) and An(IV) (An = Th, Np, Pu), the formation of highly charged anionic hydrolysis species in concentrated alkaline $CaCl_2$ solutions is stabilized by the contribution of Ca^{2+} in the second coordination sphere of the tetravalent cation.[21,35,36] The number of Ca^{2+} ions participating in the complex formation was inferred from model calculations and EXAFS spectroscopy for Zr(IV) and Th(IV), and was based on the analogy with Th(IV) in the case of Np(IV) and Pu(IV). In this work, the stability of the $Ca_n[TcO(OH)_5]^{2n-3}$ species (n = 1–3) was evaluated by large-scale DFT calculations. In order to understand the role of Ca^{2+} in the stabilization of the highly charged $[TcO(OH)_5]^{3-}$ moiety, the stability of the latter in the absence of Ca^{2+} ions was also investigated.

DFT calculations show that only the $Ca_3[TcO(OH)_5]^{3+}$ species is stable both in the gas phase and enwrapped by one hundred water molecules (Fig. 9). In contrast, the $Ca[TcO(OH)_5]^-$, $Ca_2[TcO(OH)_5]^+$ and $[TcO(OH)_5]^{3-}$ species break apart both in the gas and aqueous phases, mostly due to the insufficient or inexistent charge compensation of the $[TcO(OH)_5]^{3-}$ moiety. Tc(IV)–Ca distances optimized by DFT for the $Ca_3[TcO(OH)_5]^{3+}$ species enwrapped by one hundred water molecules (R_{Tc-Ca1} = 3.01 Å, R_{Tc-Ca2} = 3.11 Å, R_{Tc-Ca3} = 3.33 Å; average R_{Tc-Ca} = 3.15 Å) are in line with distances determined by EXAFS for Zr(IV)–Ca (R = 3.38 ± 0.02 Å) and Th(IV)–Ca (R = 3.98 ± 0.02 Å) in $Ca_3[Zr(OH)_6]^{4+}$ and $Ca_4[Th(OH)_8]^{4+}$, respectively.‡,[40] The outcome of these theoretical calculations supports the predominance of the $Ca_3[TcO(OH)_5]^{3+}$ species in concentrated $CaCl_2$ systems, which otherwise cannot be assessed by spectroscopic means. The quantum chemical and DFT studies performed will be presented in more detail in a separate manuscript by R. Polly *et al.* currently under preparation.

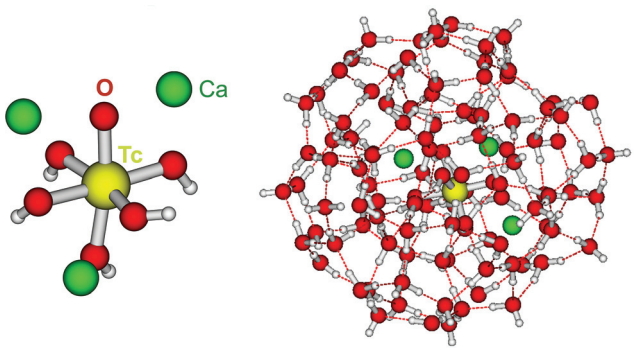

Fig. 9 Optimized structure of the complex $Ca_3[TcO(OH)_5]^{3+}$ as calculated by DFT in the gas phase, and complex enwrapped by 100 water molecules.

4 Tc(IV) chemical, thermodynamic and activity models

Chemical models describing the aquatic chemistry and relevant equilibrium reactions of Tc(IV) in dilute to concentrated NaCl, $MgCl_2$ and $CaCl_2$ are evaluated in this section based on (i) the slope analyses ($\log m_{Tc}$ *vs.* pH_m) of experimental solubility data determined in this work, (ii) detailed solid phase characterization and identification of solubility controlling compounds, (iii) spectroscopic (XANES, EXAFS) evidence gained in this work and previously reported in the literature, and (iv) the new structural information obtained by DFT calculations. After deriving the chemical model and defining the relevant equilibrium reactions for a given system, conditional solubility constants ($\log K'_s$) are determined for each investigated ionic strength, and extrapolated to I = 0 using both SIT and Pitzer activity models. SIT and Pitzer ion interaction coefficients are gained in the process of extrapolation conditional data to I = 0. Calculation of uncertainties throughout the com-

‡The same trend is reported for the ionic radii of the corresponding metal cations: Tc(IV) = 0.645 Å (CN = 6), Zr(IV) = 0.72 Å (CN = 6), Th(IV) = 1.05 Å (CN = 8).[48]

plete process is based on the NEA guidelines for the assignment of uncertainties.[41]

4.1 Acidic pH conditions ($pH_m \leq 4$)

Independent of the background electrolyte, the solubility of Tc(IV) in the acidic pH region systematically increases with increasing ionic strength. The increase of the solubility is very similar in NaCl and $MgCl_2$ solutions of analogous ionic strength. The slope ($\log m_{Tc}$ *vs.* pH_m) of −2 defined by solubility data under acidic conditions with 0.1 M ≤ I ≤ 13.5 M indicates that $2H^+$ are consumed in the chemical reaction controlling the solubility of Tc in this pH region. The combination of solvent extraction and XANES analysis confirms that no oxidation of Tc(IV) occurred in the aqueous or solid phases during the timeframe of the study. A pH-independent solubility behaviour is observed in 4.5 M $MgCl_2$ systems with $pH_m \leq$ 3.5. EXAFS characterization of the aqueous phase under these m_{Cl^-} and pH_m conditions confirms the presence of Cl-atoms in the first coordination sphere of Tc, thus supporting the formation of Tc(IV) chloro-complexes (see section 3.4.3). Although the equilibrium Tc(IV)–O/OH–Cl(s) ⇔ Tc(IV)–O/OH–Cl(aq) is suspected to control the aqueous chemistry of Tc(IV) under these conditions (see also discussion in Hess *et al.*, 2004[7]), solubility data determined in 4.5 M $MgCl_2$ and $pH_m \leq 2$ have been disregarded in the chemical and thermodynamic models derived in this section and are omitted in the following discussion.

Provided the solubility-control exerted by $TcO_2{\cdot}0.6H_2O(s)$ (see sections 3.4.2 and 3.4.3), the slope of −2 defined by solubility data in acidic dilute to concentrated NaCl and $MgCl_2$ solutions is consistent with the predominance of the $Tc_nO_m(OH)^{2+}_{(2-4n+2m)}$ species in the aqueous phase. Although NEA–TDB (consistently with previous publications) defined the formation of the TcO^{2+} species in this pH region, more recent spectroscopic studies strongly hint towards the predominance of cationic polynuclear Tc(IV) species.[12–16] Based on the analogy with Mo(IV) and the proven formation of the cluster $Mo_3O_4{\cdot}9H_2O^{4+}$, Vichot and co-workers[13] proposed the formation of the trimeric $Tc_3O_4^{4+}$ species at pH ≤ 3. The predominance of trimeric Zr(IV) species was also favoured by Altmaier *et al.* (2008) to explain the solubility behaviour of $Zr(OH)_4(s)$ under acidic pH conditions.[21] In view of the available experimental evidence and in analogy with Mo(IV) and Zr(IV), the predominance of the trimeric $Tc_3O_5^{2+}$ species in the acidic pH region is proposed in the present work. Note that the formation/predominance of other polyatomic species such as $Tc_2O_3^{2+}$ or $Tc_4O_7^{2+}$ is also consistent with the available solubility data and spectroscopic evidence, but has been disregarded in the chemical model derived in this work. The formation of the $TcO(OH)^+$ species is not needed to properly explain the experimentally determined solubility data, and has been also disregarded in the chemical model considered in this work. The predominance of the latter species under acidic conditions was claimed by Hess and co-workers,[7] but the large stability field proposed by the authors for $TcO(OH)^+$ is ruled out in the present work due to the relevant experimental shortcomings discussed in section 3.1.

Besides the formation of $Tc_3O_5^{2+}$, the very large increase in solubility (>5 orders of magnitude!) between solubility data in dilute and concentrated chloride media may hint towards the formation of Tc(IV)–O/OH–Cl aqueous complexes in concentrated chloride solutions also beyond $pH_m > 4$. Previous spectroscopic studies[16] confirmed the predominance of the $TcCl_5(H_2O)^-$ and $Tc_2OCl_{10}^{4-}$ species in 3.0 M NaCl solutions with pH < 1.1. Above this pH, the authors proposed the predominance of a polyatomic oxo-cation $Tc_nO_y^{4n-2y}$. In the present work, the formation of Tc(IV)–O/OH–Cl aqueous complexes in 4.5 M $MgCl_2$ solutions with $pH_m \leq 4$ is also hinted by EXAFS. Besides this spectroscopic evidence, Tc(IV) solubility data follows a well-defined slope of −2 both in dilute and concentrated chloride solutions, thus indicating that the number of H^+ involved in the solubility reaction is the same in both cases. Provided the proposed predominance of the $Tc_3O_5^{2+}$ species under acidic conditions with low m_{Cl^-}, the possible formation of Tc(IV) chloro-complexes of the type $Tc_3O_5Cl_m^{(2-m)}$ with $1 \leq m \leq 4$ was also considered in the development of the chemical model. Thus, chemical reactions (1) and (2) are taken into account for the assessment of Tc(IV) solubility under acidic conditions:

$$TcO_2{\cdot}0.6H_2O(s) + 2/3\ H^+ \Leftrightarrow 1/3\ Tc_3O_5^{2+} + 0.93H_2O(l) \quad (1)$$

$$TcO_2 \cdot 0.6H_2O(s) + 2/3\ H^+ + m/3Cl^- \Leftrightarrow 1/3\ Tc_3O_5Cl_m^{(2-m)} + 0.93H_2O(l) \quad (2)$$

with

$$\log K'_{s,Tc_3O_5^{2+}} = 1/3 \log\left[Tc_3O_5^{2+}\right] - 2/3 \log[H^+] \quad (3)$$

$$\log K^\circ_{s,Tc_3O_5^{2+}} = \log K'_{s,Tc_3O_5^{2+}} + 1/3 \log \gamma_{s,Tc_3O_5^{2+}} - 2/3 \log \gamma_{H^+} + 0.93 \log a_{H_2O} \quad (4)$$

$$\log K'_{s,Tc_3O_5Cl_m^{(2-m)}} = 1/3 \log\left[Tc_3O_5Cl_m^{2-m}\right] - 2/3 \log[H^+] - m/3 \log[Cl^-] \quad (5)$$

$$\log K^\circ_{s,Tc_3O_5Cl_m^{(2-m)}} = \log K'_{s,Tc_3O_5Cl_m^{2-m}} + 1/3 \log \gamma_{s,Tc_3O_5Cl_m^{2-m}} - 2/3 \log \gamma_{H^+} - m/3 \log \gamma_{Cl^-} + 0.93 \log a_{H_2O} \quad (6)$$

In the first step, different chemical models involving the formation of $Tc_3O_5^{2+}$ and $Tc_3O_5Cl_m^{(2-m)}$ complexes were evaluated using the SIT approach. Then, the chemical model chosen was used to fit the corresponding conditional equilibrium constants with the Pitzer approach to derive $\log K_s^\circ$ and ion interaction parameters.

4.1.1 SIT approach. Three different approaches were used to assess the validity of the chemical models involving the formation of $Tc_3O_5^{2+}$ and $Tc_3O_5Cl_m^{(2-m)}$ complexes:

1. only the formation of $Tc_3O_5^{2+}$ was considered to explain Tc(IV) solubility data in dilute to concentrated NaCl and $MgCl_2$ solutions.

2. Formation of both $Tc_3O_5^{2+}$ and $Tc_3O_5Cl_m^{(2-m)}$ with $1 \le m \le 4$ was considered to explain Tc(IV) solubility data in dilute to concentrated NaCl and $MgCl_2$ solutions:

a. Use of Tc(IV) solubility data at low ionic strength (0.1 M NaCl) and $\varepsilon(Tc_3O_5^{2+}, Cl^-) = (0.15 \pm 0.1)$ kg mol^{-1} estimated according to charge analogies[42] to determine $\log K^\circ_{s,Tc_3O_5^{2+}}$. Solubility data not explained by the contribution of this species are then fitted assuming the formation of $Tc_3O_5Cl_m^{(2-m)}$. Four independent models (including the formation of Tc(IV) chloro-complexes with $1 \le m \le 4$) are evaluated.

b. Use of Tc(IV) solubility data at $[Cl^-] \le 3.0$ M to determine $\log K^\circ_{s,Tc_3O_5^{2+}}$ and $\varepsilon(Tc_3O_5^{2+}, Cl^-)$, and data at $[Cl^-] > 3.0$ M to determine $\log K^\circ_{s,Tc_3O_5Cl_m^{2-m}}$ and $\varepsilon(Tc_3O_5Cl_m^{(2-m)}, Na^+/Cl^-)$.

Approach 2a properly explains Tc(IV) solubility data in dilute to concentrated NaCl and $MgCl_2$ solutions (data not shown). However, this approach suggests the predominance of $Tc_3O_5Cl_m^{(2-m)}$ complexes at $[Cl^-] \ge 0.5$ M. This is in strong contradiction with previous spectroscopic observations, which confirmed the predominance of $Tc_nO_y^{4n-2y}$ in NaCl systems with $[Cl^-] \le 3.0$ M and pH > 1.1.

Approach 2b clearly overestimates the solubility of Tc(IV) (data not shown). Hence, $\log K^\circ_{s,Tc_3O_5^{2+}}$ and $\varepsilon(Tc_3O_5^{2+}, Cl^-)$ derived from solubility data at $[Cl^-] \le 3.0$ M are able to perfectly explain experimental observations gained up to $[Cl^-] = 9.0$ M. Any additional contribution to the solubility provided by the definition of $Tc_3O_5Cl_m^{(2-m)}$ species results in the overestimation of $m_{Tc(IV)}$ in equilibrium with $TcO_2{\cdot}0.6H_2O$(s). The outcome of approach 2b further indicates that the chemical model in approach 1 is the only one consistent with both solubility in dilute to concentrated NaCl and $MgCl_2$ systems and spectroscopic observations available in the literature.[12,17]

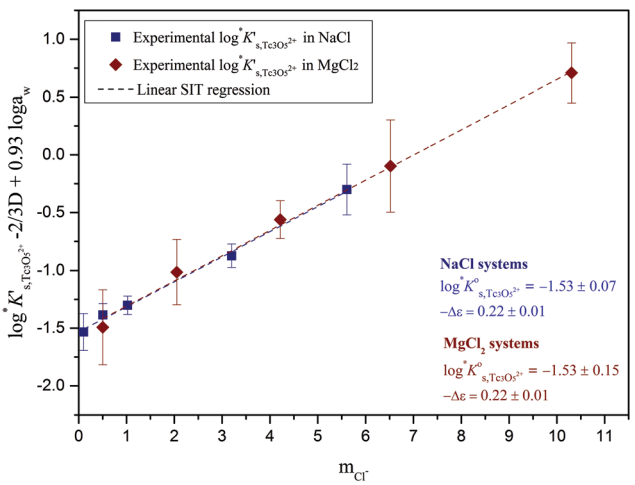

Fig. 10 SIT-plot for the solubility reaction $TcO_2{\cdot}0.6H_2O$(s) + 2/3 $H^+ \Leftrightarrow$ 1/3 $Tc_3O_5^{2+}$ + 0.93H_2O(l) considering experimental $\log K'_{s,Tc_3O_5^{2+}}$ determined in dilute to concentrated NaCl and $MgCl_2$ solutions.

Fig. 10 shows the perfect agreement between the SIT-plots derived for NaCl and $MgCl_2$ systems considering the only formation of $Tc_3O_5^{2+}$. This observation supports again that the same chemical model applies to dilute and concentrated chloride systems, and further that the formation of Tc(IV)–O/OH–Cl complexes can be disregarded under these pH_m and m_{Cl^-} conditions.

The *y*-intercept and slope determined by linear regression of the SIT-plots in Fig. 10 correspond to $\log K^\circ_{s,Tc_3O_5^{2+}}$ and $-\Delta\varepsilon$ (with $-\Delta\varepsilon = -1/3\ \varepsilon(Tc_3O_5^{2+}, Cl^-) + 2/3\ \varepsilon(H^+, Cl^-)$), respectively. The combination of $-\Delta\varepsilon$ and $\varepsilon(H^+, Cl^-)$ reported in the NEA–TDB further allows the calculation of $\varepsilon(Tc_3O_5^{2+}, Cl^-)$. Excellent agreement is found between $\log K^\circ_{s,Tc_3O_5^{2+}}$ and $\varepsilon(Tc_3O_5^{2+}, Cl^-)$ derived from NaCl and $MgCl_2$ systems. The final selection gained in this work is:

$$\log K^\circ_{s,Tc_3O_5^{2+}} = -(1.53 \pm 0.15)$$
$$\varepsilon(Tc_3O_5^{2+}, Cl^-) = -(0.42 \pm 0.05) \text{ kg mol}^{-1}$$

The SIT ion interaction coefficient determined for $Tc_3O_5^{2+}$ is much lower than that expected for a typical divalent cation according with charge-based correlations ($\varepsilon(M^{2+}, Cl^-) = 0.15 \pm 0.10$ kg mol^{-1}).[42] However, the use of charge analogies for very large or oligomeric species must be considered with caution. The effect of size and the distribution of the formal charge throughout the voluminous species can lead to large deviations with respect to monomeric/simple species. Similar effects are observed for ternary Ca–M–OH complexes, as discussed in section 4.4.

4.1.2 Pitzer approach. Conditional solubility constants determined in NaCl and $MgCl_2$ systems according to eqn (3) were also fitted following the Pitzer formalism. The values of $\log \gamma_{H^+}$ and a_w in eqn (4) are calculated from the parameters reported by Harvie *et al.*[43] The binary parameter $\beta^{(2)}$ is only $\neq 0$ for 2–2 electrolytes. The mixing parameters $\theta(Tc_3O_5^{2+}, Na^+)$ and $\Psi(Tc_3O_5^{2+}, Cl^-, Na^+)$ are set to zero. $\log K^\circ_{s,Tc_3O_5^{2+}}$, $\beta^{(0)}$, $\beta^{(1)}$ and C^Φ are fitted simultaneously for NaCl and $MgCl_2$ systems by minimizing the difference between experimental and modelled $\log K'_{s,Tc_3O_5^{2+}}$ in both systems. The resulting values are:

$$\log K^\circ_{s,Tc_3O_5^{2+}} = -(1.50 \pm 0.10) \quad \beta^{(0)} = -0.3681 \text{ kg mol}^{-1}$$
$$\beta^{(1)} = 2.6972 \text{ kg mol}^{-1} \quad C^\Phi = 0.0063 \text{ kg}^2 \text{ mol}^{-2}$$

$\log K^\circ_{s,Tc_3O_5^{2+}}$ values derived using both SIT and Pitzer approaches are in excellent agreement. The value of $\beta^{(0)}$ resulting from the Pitzer fit is also in good agreement with the estimate calculated following the approach described by Grenthe *et al.*[44] ($\beta^{(0)} = -0.32$ kg mol^{-1}).§

Fig. 11 compares the experimental and calculated $\log K'_{s,Tc_3O_5^{2+}}$ for NaCl and $MgCl_2$ systems, using both SIT and Pitzer approaches. The figure clearly shows that both activity models describe very well experimentally determined $\log K'_{s,Tc_3O_5^{2+}}$

§ $\beta^{(0)}_{MX} = 0.15 + \varepsilon(M,X){\cdot}(\ln 10)/2$ for $M^{2+} - X^-$ interactions, where $\varepsilon(M,X)$ is the SIT ion interaction coefficient determined for the same species.

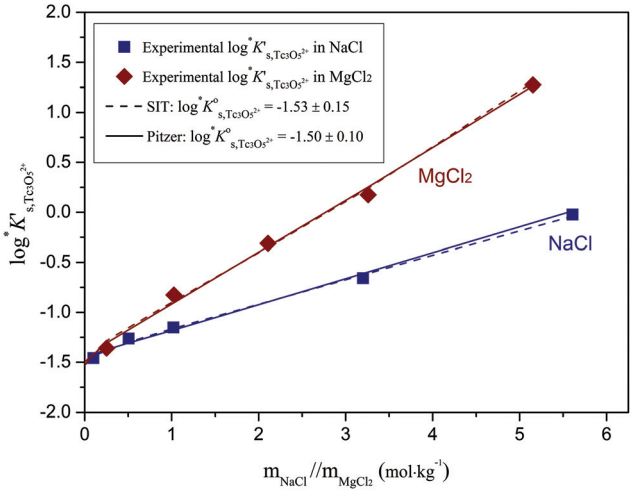

Fig. 11 Conditional equilibrium constants $\log K'_{s,Tc_3O_5^{2+}}$ as a function of NaCl and $MgCl_2$ molalities: experimental values (symbols) and calculated functions based on the SIT (dashed line) and Pitzer models (solid line).

values in dilute to concentrated saline systems, confirming again the good performance of SIT well beyond $I_m > 3.5$ m.

4.2 Weakly acidic to weakly alkaline pH conditions ($4 \leq pH_m \leq 8/11$)

The solubility of Tc(IV) follows a pH-independent behaviour at $4 \leq pH_m \leq 11$ and $4 \leq pH_m \leq 8$ in NaCl and $MgCl_2$ or $CaCl_2$ systems, respectively. Provided a solubility-control by $TcO_2{\cdot}0.6H_2O(s)$, this observation indicates that a neutral hydrolysis species prevails in the aqueous phase within this pH range. Tc(IV) solubility shows no ionic strength dependency within this pH region, in good agreement with the behaviour expected for neutral species. Based on the available experimental evidence and consistently with the NEA–TDB[18] selection, chemical reaction (7) is defined for the control of Tc(IV) solubility within this pH region.

$$TcO_2{\cdot}0.6H_2O(s) + 0.4H_2O(l) \Leftrightarrow TcO(OH)_2(aq) \quad (7)$$

with

$$\log K'_{s,TcO(OH)_{2(aq)}} = \log [TcO(OH)_2(aq)] \quad (8)$$

$$\log K^{\circ}_{s,TcO(OH)_{2(aq.)}} = \log K'_{s,TcO(OH)_{2(aq.)}} + \log \gamma_{TcO(OH)_{2(aq.)}} - 0.4 \log a_{H_2O} \quad (9)$$

SIT and Pitzer ion interaction coefficients for the neutral $TcO(OH)_2(aq)$ species are considered equal to zero. Thus, $\log K^{\circ}_{s,TcO(OH)_{2(aq.)}}$ is calculated as the average m_{Tc} measured within $4 \leq pH_m \leq 11$, accounting also for the small contribution of water activity in eqn (9). The resulting value ($\log K^{\circ}_{s,TcO(OH)_2(aq.)} = -8.8 \pm 0.5$) is slightly lower but agrees within the uncertainty with the current NEA–TDB selection ($\log K^{\circ}_{s,TcO(OH)_2(aq.)} = -8.4 \pm 0.5$).

Note that the formation and predominance of polyatomic species of the type $Tc_nO_m(OH)_{4n-2m}(aq)$ are also consistent with the available experimental evidence. Although the definition of the monomeric $TcO(OH)_2(aq)$ species is favoured in the present work in agreement with the NEA–TDB selection, a definitive proof-of-concept for the predominance of this species is still missing.

4.3 Alkaline pH conditions ($pH_m \geq 11$) in NaCl system

Solubility data of Tc(IV) in dilute to concentrated NaCl solutions with $pH_m \geq 11$ follow a well-defined slope of +1. Considering a solubility-control by $TcO_2{\cdot}0.6H_2O(s)$, this observation is properly explained by the predominance in the aqueous phase of the $TcO(OH)_3^-$ species. This chemical model is consistent with the current NEA–TDB[18] selection:

$$TcO_2 \cdot 0.6H_2O(s) + 1.4H_2O(l) \Leftrightarrow TcO(OH)_3^- + H^+ \quad (10)$$

with

$$\log K'_{s,TcO(OH)_3^-} = \log[TcO(OH)_3^-] + \log[H^+] \quad (11)$$

$$\log K^{\circ}_{s,TcO(OH)_3^-} = \log K'_{s,TcO(OH)_3^-} + \log \gamma_{s,TcO(OH)_3^-} + \log \gamma_{H^+} - 1.4 \log a_{H_2O} \quad (12)$$

Conditional solubility constants ($\log K'_{s,TcO(OH)_3^-}$) are determined based on experimental solubility data in 0.1–5.0 M NaCl according to eqn (11). The use of eqn (12) allows the extrapolation of $\log K'_{s,TcO(OH)_3^-}$ to $I = 0$ and the determination of the corresponding SIT/Pitzer ion interaction parameters.

4.3.1 SIT approach. Eqn (12) is further extended with the calculation of $\gamma_{s,TcO(OH)_3^-}$ and γ_{H^+} according to the SIT formalism:

$$\log K'_{s,TcO(OH)_3^-} - 2D - 1.4 \log a_w = \log K^{\circ}_{s,TcO(OH)_3^-} - \left[\varepsilon(TcO(OH)_3^-, Na^+) + \varepsilon(H^+, Cl^-)\right] \cdot m_{NaCl} \quad (13)$$

The linear regression ($\log K'_{s,TcO(OH)_3^-} - 2D - 1.4 \log a_w$) *vs.* m_{NaCl} (SIT-plot) is shown in Fig. 12. The resulting solubility

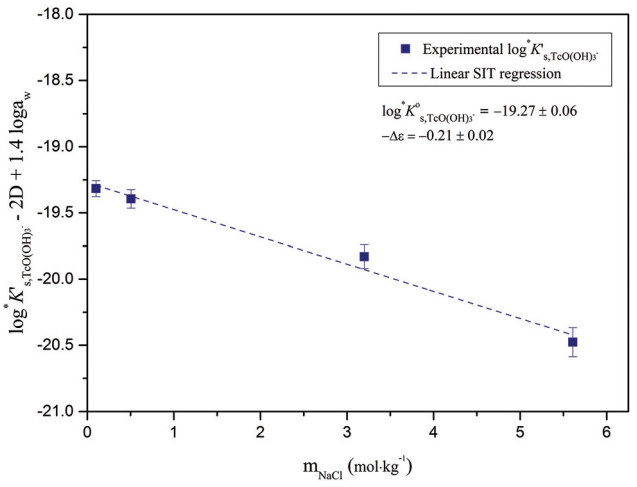

Fig. 12 SIT-plot for the solubility reaction $TcO_2{\cdot}0.6H_2O(s) + 1.4H_2O(l) \Leftrightarrow TcO(OH)_3^- + H^+$ considering experimental $\log K'_{s,TcO(OH)_3^-}$ determined in dilute to concentrated NaCl solutions.

constant at I = 0, $\log K^{\circ}_{s,TcO(OH)_3^-} = -19.27 \pm 0.06$, is in excellent agreement with the current NEA–TDB selection ($\log K^{\circ}_{s,TcO(OH)_3^-} = -19.3 \pm 0.6$), and represents a very significant contribution in decreasing the associated uncertainty. The ion interaction coefficient $\varepsilon(TcO(OH)_3^-, Na^+)$ = (0.09 ± 0.02) kg mol^{-1} is calculated from the slope of the linear regression ($-\Delta\varepsilon = -\varepsilon(TcO(OH)_3^-, Na^+) - \varepsilon(H^+, Cl^-)$ = (−0.21 ± 0.02) kg mol^{-1}), considering $\varepsilon(H^+, Cl^-)$ = (0.12 ± 0.01) kg mol^{-1} as reported by Guillaumont *et al.* (2003).[18] This value is in moderate agreement with SIT ion interaction coefficients expected for a typical monovalent anion $\varepsilon(X^-, Na^+) = -(0.05 \pm 0.10)$ kg mol^{-1}.[42] Note that positive SIT ion interaction coefficients have been previously reported for anionic hydrolysis species of metal cations with similar ionic radii (*e.g.* Zr,[21] Sn[45]).

4.3.2 Pitzer approach. Conditional solubility constants determined in alkaline NaCl systems were also fitted according to eqn (11) and considering the Pitzer formalism. The binary parameter $\beta^{(2)}$ and the mixing parameters $\theta(TcO(OH)_3^-, Cl^-)$ and $\Psi(TcO(OH)_3^-, Cl^-, Na^+)$ are set to zero. $\beta^{(1)}$ is set to 0.3 based on charge analogies reported elsewhere.[44] $\log K^{\circ}_{s,TcO(OH)_3^-}$, $\beta^{(0)}$ and $C^{(\Phi)}$ are fitted by minimizing the difference between experimental and modelled $\log K'_{s,TcO(OH)_3^-}$ in 0.1 M, 0.5 M, 3.0 M and 5.0 M NaCl systems, and resulted in:

$$\log K^{\circ}_{s,TcO(OH)_3^-} = -(19.32 \pm 0.10) \quad \beta^{(0)} = -0.0087 \text{ kg mol}^{-1}$$
$$\beta^{(1)} = 0.30 \text{ kg mol}^{-1} \quad C^{(\Phi)} = 0.035 \text{ kg}^2 \text{ mol}^{-2}$$

Excellent agreement is obtained between $\log K^{\circ}_{s,TcO(OH)_3^-}$ values determined using SIT and Pitzer approaches. The extrapolation of this value to higher ionic strengths using the Pitzer activity model derived in this work results in a very good agreement with experimental $\log K'_{s,TcO(OH)_3^-}$ (Fig. 13). In the case of SIT, minor deviations (≈ 0.1 log-units) appear between experimental and calculated $\log K'_{s,TcO(OH)_3^-}$ at [NaCl] ≥ 3.0 M.

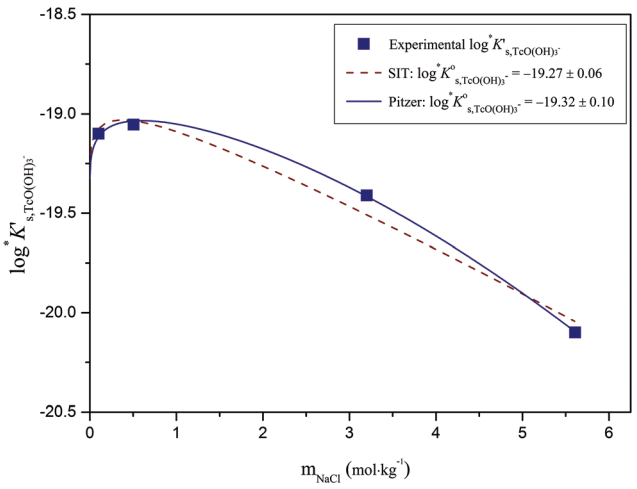

Fig. 13 Conditional equilibrium constants $\log K'_{s,TcO(OH)_3^-}$ as a function of NaCl molality; experimental values (symbols) and calculated functions based on the SIT (dashed line) and Pitzer models (solid line).

4.4 Alkaline pH conditions ($pH_m \geq 8$) in $MgCl_2$ and $CaCl_2$ systems

The solubility of Tc(IV) shows a steep increase with a slope of +3 ($\log m_{Tc}$ *vs.* pH_m) in concentrated $MgCl_2$ and $CaCl_2$ solutions with $pH_m \geq 8$ and solubility control by the $TcO_2{\cdot}0.6H_2O$ (s) phase. This observation cannot be explained assuming the only formation of the $TcO(OH)_3^-$ species, and requires extending the chemical model so far available for Tc(IV) under alkaline conditions. Because of the pH-limitations in $MgCl_2$ systems caused by the precipitation of $Mg(OH)_2$(s) or Mg–OH–Cl(s) ($pH_{max} \approx 9$), chemical, thermodynamic and activity models for MCl_2 systems (M = Mg, Ca) were first derived for $CaCl_2$ where a significantly larger pH range can be assessed.

The slope of +3 observed in the experimental solubility data indicates the release of $3H^+$ in the chemical reaction controlling the solubility of Tc(IV) in systems with $[CaCl_2] \geq 1.0$ M and $pH_m \geq 8$. Provided the predominance of the solid phase $TcO_2{\cdot}0.6H_2O$(s), a new aqueous species holding the moiety $[TcO(OH)_5]^{3-}$ must be defined. Experimental data collected in NaCl–NaOH systems strongly argue for $TcO(OH)_3^-$ as limiting hydrolysis species forming under alkaline to hyperalkaline pH conditions. The moiety $[TcO(OH)_5]^{3-}$ has not been reported in NaCl media and is thus specifically stabilized by Ca^{2+} or Mg^{2+}, either involving the formation of ternary species of the type $Ca_n/Mg_n[TcO(OH)_5]^{2n-3}$ or by strong ion interaction processes. Previous studies focussing on the solubility of Ln(III), An(III/IV/V) and Zr(IV) in concentrated $CaCl_2$ systems have provided unequivocal indications on the formation of ternary Ca–Ln/An/Zr–OH complexes under alkaline pH conditions.[21,34,35,46] In most cases, the formation of these species was accompanied by the full occupancy of the coordination sphere of the central metal atom, as also occurs in the moiety $[TcO(OH)_5]^{3-}$ ($CN_{Tc(IV)}$ = 6). Based on the previous evidence available for An(IV) and Zr(IV), the formation of ternary complexes of the type $Ca_nTcO(OH)_5^{(2n-3)}$ in concentrated $CaCl_2$ solutions is postulated for Tc(IV). The chemical reaction (14) is thus proposed to control the solubility of Tc(IV) under these conditions:

$$TcO_2{\cdot}0.6H_2O(s) + nCa^{2+} + 3.4H_2O(l) \Leftrightarrow Ca_nTcO(OH)_5^{(2n-3)} + 3H^+ \quad (14)$$

with

$$\log K'_{s,Ca_nTcO(OH)_5^{(2n-3)}} = \log\left[Ca_nTcO(OH)_5^{(2n-3)}\right] + 3\log[H^+] - n\log[Ca^{2+}] \quad (15)$$

$$\log K^{\circ}_{s,Ca_nTcO(OH)_5^{(2n-3)}} = \log K'_{s,Ca_nTcO(OH)_5^{(2n-3)}} + \log\gamma_{s,Ca_nTcO(OH)_5^{(2n-3)}} + 3\log\gamma_{H^+} - n\log\gamma_{Ca^{2+}} - 3.4\log a_{H_2O} \quad (16)$$

Conditional stability constants for reaction (14) are determined according to eqn (15) from Tc(IV) experimental solubility data gained in 1.0 M, 2.0 M and 4.5 M $CaCl_2$ systems. The value of $\log K^{\circ}$ is calculated by extrapolating the results in high

ionic strength to $I = 0$ according to eqn (16). DFT calculations support the formation and stability of ternary complexes of the type $Ca_nTcO(OH)_5^{(2n-3)}$ with $n = 3$ (see section 3.4.4). In spite of this and to gain further confidence in the chemical model controlling the chemistry of Tc under these conditions, Tc(IV) solubility data in concentrated [$CaCl_2$] systems with $pH_m \geq 8$ have been evaluated considering four different chemical models based on eqn (16) with n = 1–4 to justify the quality of the adopted chemical model. Although it is postulated that the stabilization of the moiety [$TcO(OH)_5^{3-}$] requires the formation of a new aqueous complex involving the participation of Ca^{2+}, the fifth case with $n = 0$ is also evaluated for comparison purposes. In the first step, $\log K^\circ$ values and ion interaction coefficients are calculated using the SIT approach. In the second step, the best chemical model selected accordingly with the criteria described below, was used to derive $\log K^\circ_{s,Ca_nTcO(OH)_5^{(2n-3)}}$ and ion interaction coefficients according to the Pitzer formalism.

4.4.1 SIT approach. Five different sets of $\log K_{s,Ca_nTcO(OH)_5^{(2n-3)}}$ are calculated according to eqn (14) and considering n = 0–4 (Table 5). The use of SIT for the determination of $\log K^\circ_{s,Ca_nTcO(OH)_5^{(2n-3)}}$ involves the linear regression of $(\log K'_{s,Ca_nTcO(OH)_5^{(2n-3)}} - mD - 3.4\log a_w)$ *vs.* m_{CaCl_2} (see Fig. A2†). The SIT ion interaction coefficient of the forming species $\varepsilon(Ca_n[TcO(OH)_5]^{2n-3}, Ca^{2+}/Cl^-)$ can be calculated from the slope of the linear regression ($-\Delta\varepsilon$) in combination with $\varepsilon(H^+, Cl^-) = (0.12 \pm 0.01)$ kg mol^{-1} and $\varepsilon(Ca^{2+}, Cl^-) = (0.14 \pm 0.01)$ kg mol^{-1} as reported in the NEA–TDB.[18]

Table 5 summarizes $\log K^\circ_{s,Ca_nTcO(OH)_5^{(2n-3)}}$ and $\varepsilon(Ca_n[TcO(OH)_5]^{2n-3}, Ca^{2+}/Cl^-)$ determined for the five chemical models evaluated, involving the formation of the binary/ternary $Ca_nTcO(OH)_5^{(2n-3)}$ species with n = 0–4. Table 5 also shows the "quality parameter" (Δ), which is calculated as $\sum \left| \log K'^{,exp}_{s,Ca_nTcO(OH)_5^{(2n-3)}} - \log K'^{,calc}_{s,Ca_nTcO(OH)_5^{(2n-3)}} \right|^2$ and analyses the goodness of the fit. The final selection of the chemical model for Tc(IV) in concentrated alkaline $CaCl_2$ solutions is based on the criteria described below. Note that a similar strategy was successfully applied by Fellhauer for the evaluation of the ternary system Ca–Np(V)–OH in dilute to concentrated $CaCl_2$ solutions.[46,47]

– Minimization of the "quality parameter" (Δ, Table 5).

– Consistency of SIT ion interaction coefficients. $\varepsilon(i,j)$ are known to correlate with the charge of the ion,[42] although significant deviations from this trend are expected for polyatomic species or voluminous ternary complexes. $\varepsilon(Ca_n[TcO(OH)_5]^{2n-3}, Ca^{2+}/Cl^-)$ values calculated in the present work (Table 5) are compared with $\varepsilon(i,j)$ values reported for Ca–An(III/IV/V)–OH and Ca–Zr(IV)–OH complexes.

– Shape of the plot $\log K_{s,Ca_nTcO(OH)_5^{(2n-3)}}$ *vs.* $CaCl_2$ concentration. The plot should give a smooth shape without jumps or turning points (Fig. A3†).

All the chemical models result in a smooth shape of the plot $\log K'_s$ *vs.* m_{CaCl_2} (Fig. A3†). Chemical models involving the formation of the $[TcO(OH)_5]^{3-}$, $Ca[TcO(OH)_5]^-$ and $Ca_4[TcO(OH)_5]^{5+}$ species led to very large and clearly unrealistic values of $\varepsilon(i,j)$ and/or Δ, and consequently were disregarded. The $Ca_2[TcO(OH)_5]^+$ species shows a relatively low Δ, but retains a very negative SIT ion interaction coefficient. The chemical model including the species $Ca_3[TcO(OH)_5]^{3+}$ species has the lowest Δ and holds a less negative SIT ion interaction coefficient ($\varepsilon(Ca_3[TcO(OH)_5]^{3+}, Cl^-) = -(0.37 \pm 0.10)$ kg mol^{-1}). The latter value is very discrepant with respect to the value estimated according to the charge-analogy concept ($\varepsilon(M^{3+},Cl^-) = (0.25 \pm 0.10)$ kg mol^{-1}). As discussed above, the applicability of charge analogies for the estimation of $\varepsilon(i,j)$ in the case of voluminous complexes has been previously challenged in the literature and is also disregarded in the present case.

Based on the discussion above and considering the clear inputs obtained from DFT calculations (see section 3.4.4), the chemical model involving the formation of the ternary $Ca_3[TcO(OH)_5]^{3+}$ species is selected in the present work.

$$\log K^\circ_{s,Ca_3TcO(OH)_5^{3+}} = -(41.53 \pm 0.30)$$
$$\varepsilon(Ca_3[TcO(OH)_5]^{3+}, Cl^-) = -(0.37 \pm 0.10) \text{ kg mol}^{-1}$$

The same chemical model is considered for the interpretation of experimental observations in concentrated $MgCl_2$ solutions with $pH_m \geq 8$. Due to limitations in pH_m caused by the precipitation of $Mg(OH)_2$(s) or Mg–OH–Cl(s) ($pH_{max} \approx 9$), the increase of Tc(IV) solubility with the slope of +3 is only observed in 4.5 M $MgCl_2$. This allows the only calculation of $\log K'_{s,Mg_3TcO(OH)_5^{3+}}$ for this ionic strength. In order to overcome

Table 5 $\log K'$ values determined from Tc(IV) solubility data in 1.0, 2.0 and 4.5 M $CaCl_2$ according to chemical reaction (14) and eqn (15) for n = 0–4. $\log K^\circ$ and $\varepsilon(i,j)$ values determined using the linear regressions shown in the SIT-plot, Fig. A2

Species	$\log K'_{experimental}$ [a]			Outcome of SIT – plot			
I	1.0 M	2.0 M	4.5 M	$\log K^\circ$	j	$\varepsilon(i,j)$	Quality
$[TcO(OH)_5]^{3-}$	−40.70	−39.00	−36.00	−44.69 ± 0.3	Ca^{2+}	−1.93 ± 0.10	Δ = 0.10
$Ca[TcO(OH)_5]^-$	−40.71	−39.32	−36.72	−41.71 ± 0.3	Ca^{2+}	−1.61 ± 0.10	Δ = 0.10
$Ca_2[TcO(OH)_5]^+$	−40.72	−39.64	−37.44	−40.65 ± 0.3	Cl^-	−0.60 ± 0.10	Δ = 0.04
$Ca_3[TcO(OH)_5]^{3+}$	**−40.73**	**−39.97**	**−38.16**	**−41.53 ± 0.3**	**Cl^-**	**−0.37 ± 0.10**	**Δ = 0.00**
$Ca_4[TcO(OH)_5]^{5+}$	−40.74	−40.30	−38.88	−44.32 ± 0.3	Cl^-	−0.08 ± 0.20	Δ = 0.11

[a] Uncertainty of $\log K'$ values determined as ± 0.3.

the limited data set available, $\varepsilon(Mg_3[TcO(OH)_5]^{3+}, Cl^-)$ is considered $\approx \varepsilon(Ca_3[TcO(OH)_5]^{3+}, Cl^-)$, and $\log K^\circ_{s,Mg_3TcO(OH)_5^{3+}}$ is accordingly calculated using the SIT approach.

$$\log K^\circ_{s,Mg_3TcO(OH)_5^{3+}} = -(40.55 \pm 0.50)$$

This value is significantly higher than $\log K^\circ_{s,Ca_3TcO(OH)_5^{3+}}$, thus reflecting the earlier (lower pH_m values) increase in solubility observed in $MgCl_2$ systems.

4.4.2 Pitzer approach. The chemical model involving the formation of the $Ca_3[TcO(OH)_5]^{3+}$ species was also used for the extrapolation of the conditional equilibrium constants to $I = 0$ using the Pitzer formalism. $\beta^{(1)}$ was set to 4.30 as recommended in the literature for $M^{3+}:X^-$ interactions.[34,35,44] The binary parameters $\beta^{(2)}$ and the mixing parameters $\theta(Ca_3[TcO(OH)_5]^{3+}, Ca^{2+})$ and $\Psi(Ca_3[TcO(OH)_5]^{3+}, Cl^-, Ca^{2+})$ were set to zero. $\log K^\circ_{s,Ca_3TcO(OH)_5^{3+}}$ and $\beta^{(0)}$ were fitted for $CaCl_2$ systems by minimizing the difference between experimental and calculated $\log K'_{s,Ca_3TcO(OH)_5^{3+}}$ in 1.0 M, 2.0 M and 4.5 M $CaCl_2$ systems. The resulting values are:

$$\log K^\circ_{s,Ca_3TcO(OH)_5^{3+}} = -(41.65 \pm 0.30) \quad \beta^{(0)} = -0.074 \text{ kg mol}^{-1}$$
$$\beta^{(1)} = 4.30 \text{ kg mol}^{-1} \quad C^{(\Phi)} = 0.015 \text{ kg}^2 \text{ mol}^{-2}$$

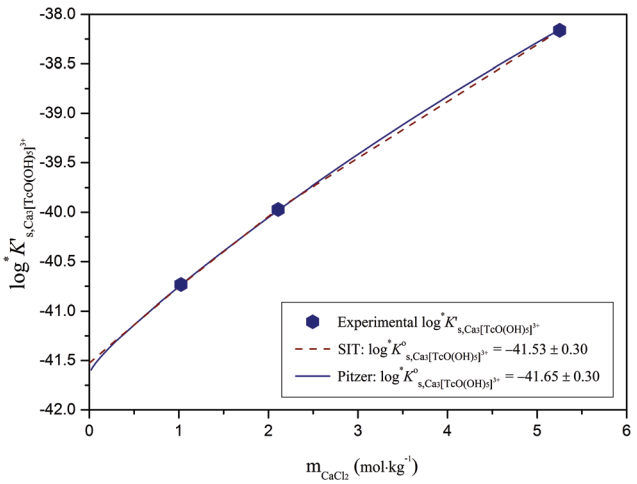

Fig. 14 Conditional equilibrium constants $\log K'_{s,Ca_3TcO(OH)_5^{3+}}$ as a function of $CaCl_2$ molality; experimental values (symbols) and calculated functions based on the SIT (dashed line) and Pitzer models (solid line).

The value of $\beta^{(0)}$ can also be estimated for $M^{3+}:X^-$ interactions according to $\beta^{(0)}_{MX} = 0.366 + \varepsilon_{MX}\cdot(\ln 10)/2$ [44] and using $\varepsilon(Ca_3[TcO(OH)_5]^{3+}, Cl^-) = -0.37 \pm 0.1$ kg mol^{-1} as determined in the present study. The resulting estimate ($\beta^{(0)} = -0.0599$) is in good agreement with the value obtained in the fit. Fig. 14 shows that both SIT and Pitzer models explain very well $\log K'_{s,Ca_3TcO(OH)_5^{3+}}$ values determined from the experimental solubility data.

As in the SIT approach, Pitzer ion interaction parameters determined for $Ca_3[TcO(OH)_5]^{3+}$ are used for $Mg_3[TcO(OH)_5]^{3+}$ to extrapolate the conditional stability constant at 4.5 M $MgCl_2$ to $I = 0$ and to calculate $\log K^\circ_{s,Mg_3TcO(OH)_5^{3+}} = -(40.32 \pm 0.50)$. This value agrees within their uncertainties with $\log K^\circ_{s,Mg_3TcO(OH)_5^{3+}}$ determined using the SIT approach.

4.5 Chemical, thermodynamic and activity models for the system Tc^{4+}–Na^+–Mg^{2+}–Ca^{2+}–H^+–Cl^-–OH^-–H_2O

Tables 6 and 7 summarize the chemical, thermodynamic and (SIT/Pitzer) activity models derived in the present work for the system Tc^{4+}–Na^+–Mg^{2+}–Ca^{2+}–H^+–Cl^-–OH^-–H_2O. Fig. 15–17 show all experimental solubility data determined in the present work in dilute to concentrated NaCl, $MgCl_2$ and $CaCl_2$ systems, respectively, in combination with thermodynamic calculations performed using the SIT and Pitzer activity models summarized in Tables 6 and 7. The figures show an excellent agreement between experimental and calculated Tc(IV) solubility data, which further extends to experimental solubility data at $I \approx 0$ reported in the literature. The present work represents the first comprehensive description of Tc(IV) solubility in dilute to concentrated saline systems, covering acidic to hyperalkaline pH conditions.

5 Summary and conclusions

The solubility and speciation of Tc(IV) were successfully investigated in dilute to concentrated NaCl, $MgCl_2$ and $CaCl_2$ systems using a systematic combination of undersaturation solubility experiments, extensive solid phase characterization, aqueous speciation methods/techniques and DFT calculations. The chemical, thermodynamic and activity models accordingly derived improve and further extend the current NEA–TDB thermodynamic selection for Tc and offer the first experimentally derived comprehensive Pitzer model available for highly saline systems.

Table 6 Equilibrium constants ($I = 0$, $T = 25$ °C) determined in the present work for the solid hydrous oxide and hydrolysis species of Tc(IV)

Chemical reactions	SIT $\log K^\circ$	Pitzer $\log K^\circ$
$TcO_2{\cdot}0.6H_2O(s) + 2/3\ H^+ \Leftrightarrow 1/3Tc_3O_5^{2+} + 0.93H_2O$	−1.53 ± 0.15	−1.50 ± 0.10
$TcO_2{\cdot}0.6H_2O(s) + 0.4H_2O \Leftrightarrow TcO(OH)_2$	−8.80 ± 0.50	−8.80 ± 0.50
$TcO_2{\cdot}0.6H_2O(s) + 1.4H_2O \Leftrightarrow TcO(OH)_3^- + H^+$	−19.27 ± 0.06	−19.32 ± 0.10
$TcO_2{\cdot}0.6H_2O(s) + 3Mg^{2+} + 3.4H_2O \Leftrightarrow Mg_3[TcO(OH)_5]^{3+} + 3H^+$	−40.55 ± 0.50	−40.32 ± 0.50
$TcO_2{\cdot}0.6H_2O(s) + 3Ca^{2+} + 3.4H_2O \Leftrightarrow Ca_3[TcO(OH)_5]^{3+} + 3H^+$	−41.53 ± 0.30	−41.65 ± 0.30

Table 7 Ion interaction coefficients for Tc(IV) hydrolysis species in NaCl, $MgCl_2$ and $CaCl_2$ media at T = 25 °C. SIT ion interaction coefficents: $\varepsilon(i,j)$ in [kg mol^{-1}]; Pitzer parameters: $\beta^{(0)}_{ij}$, $\beta^{(1)}_{ij}$, λ_{ij}, $\Theta_{ii'}$ in [kg mol^{-1}], $C^{(\phi)}$ and $\Psi_{ijj'}$ in [kg^2 mol^{-2}]

Species		SIT	Pitzer				
			Binary parameters			Mixing parameters	
i	j	$\varepsilon(i,j)$	$\beta^{(0)}$	$\beta^{(1)}$	$C^{(\phi)}$	$\Theta_{ii'}$	$\Psi_{ijj'}$
$Tc_3O_5^{2+}$	Cl^-	−0.41 ± 0.05	−0.3681	2.6972	0.0063	0	0
$TcO(OH)_3^-$	Na^+	0.09 ± 0.02	−0.0087	0.3[a]	0.035	0	0
	Ca^{2+}	0.15[b]	0.3[c]	1.7[c]	0[c]	0[c]	0[c]
$Ca_3[TcO(OH)_5]^{3+}$	Cl^-	−0.37 ± 0.1	−0.074	4.3[a]	0.015	0	0
$Mg_3[TcO(OH)_5]^{3+}$	Cl^-	−0.37 ± 0.1	−0.074	4.3[a]	0.015	0	0
$TcO(OH)_2(aq)$	Na^+, Mg^{2+}, Ca^{2+}, Cl^-	0	0	0	0	0	0

[a] Fixed value for the corresponding charge type, according to ref. 44. [b] Estimated value for the corresponding charge type, according to ref. 42. [c] Estimated value for the corresponding charge type, according to ref. 48.

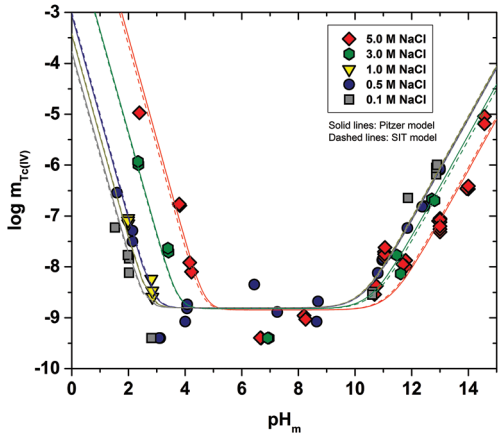

Fig. 15 Tc(IV) experimental solubility data determined in dilute to concentrated NaCl systems (symbols), and calculated solubility of $TcO_2{\cdot}0.6H_2O$(s) using the thermodynamic and (SIT/Pitzer) activity models derived in the present work.

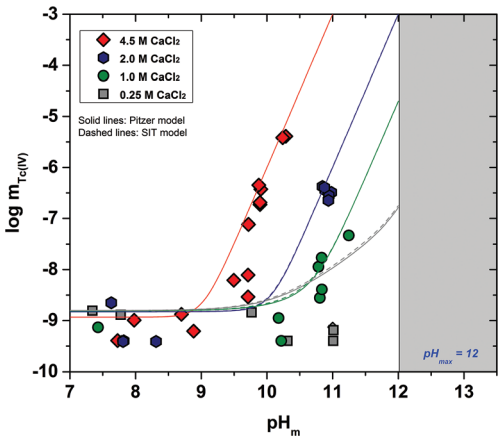

Fig. 17 Tc(IV) experimental solubility data determined in dilute to concentrated $CaCl_2$ systems (symbols), and the calculated solubility of $TcO_2{\cdot}0.6H_2O$(s) using the thermodynamic and (SIT/Pitzer) activity models derived in the present work. Shadowed area indicates the precipitation of $Ca(OH)_2$(s) ([$CaCl_2$] ≤ 2 M) or Ca–OH–Cl (s) ([$CaCl_2$] ≥ 2 M) solid phases.

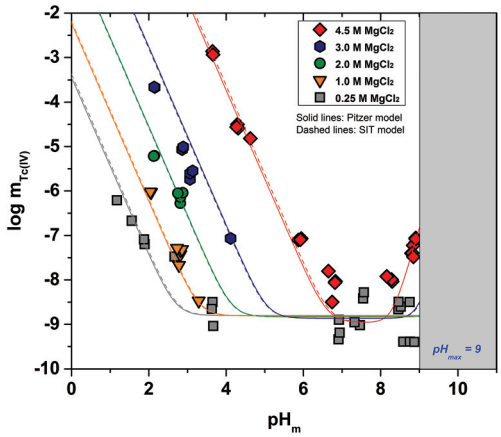

Fig. 16 Tc(IV) experimental solubility data determined in dilute to concentrated $MgCl_2$ systems (symbols), and calculated solubility of $TcO_2{\cdot}0.6H_2O$(s) using the thermodynamic and (SIT/Pitzer) activity models derived in the present work. Shadowed area indicates the precipitation of $Mg(OH)_2$(s) ([$MgCl_2$] ≤ 2 M) or Mg–OH–Cl(s) ([$MgCl_2$] ≥ 2 M).

$TcO_2{\cdot}0.6H_2O$(s) is the solid phase controlling the solubility of Tc(IV) in all the evaluated systems, except under acidic conditions with a very high chloride concentration where the formation of a Tc(IV)–Cl solid phase is hinted from solubility experiments in agreement with the literature. The previously unreported formation of the polynuclear $Tc_3O_5^{2+}$ species under acidic pH conditions is accepted based on the slope analysis of solubility data gained in the present work and spectroscopic evidence available in the literature. The predominance of this species in the aqueous phase under acidic conditions (instead of TcO^{2+} + $TcO(OH)^+$) properly explains the experimental observations from dilute to concentrated saline systems, except in very acidic systems with a high chloride concentration where the formation of binary Tc(IV)–Cl or ternary Tc(IV)–O/OH–Cl aqueous species is indicated by spectroscopic techniques. The pH-independent chemical reaction $TcO_2{\cdot}0.6H_2O(s)$ + 0.4 $H_2O(l)$ ⇔ $TcO(OH)_2(aq)$ controls the

solubility of Tc(IV) under weakly acidic to alkaline pH conditions. The stability field of $TcO(OH)_2(aq)$ decreases in concentrated saline systems due to the greater stabilization of charged species and the formation of new ternary complexes in concentrated alkaline $MgCl_2$ and $CaCl_2$ systems. $\log K^{\circ}_{s,TcO(OH)_2(aq)} = -(8.8 \pm 0.5)$ determined in the present work agrees well within the uncertainties with the value currently selected in the NEA–TDB. The solubility of Tc(IV) increases with a slope of +1 ($\log m_{Tc}$ *vs.* pH_m) in NaCl systems with $pH_m \geq 11$, indicating the predominance of $TcO(OH)_3^-$ as previously selected in the NEA–TDB and decreases about one order of magnitude with increasing ionic strength due to ion interaction processes. A very different behaviour of Tc(IV) is observed in concentrated alkaline $MgCl_2$ and $CaCl_2$ systems, where a steep increase of the solubility with a well-defined slope of +3 is observed. The formation of $Mg_3[TcO(OH)_5]^{3+}$ and $Ca_3[TcO(OH)_5]^{3+}$ species is proposed based on the slope analysis, model calculations and previous solubility and spectroscopic evidence available for An(IV) and Zr(IV). DFT calculations further support the key role of Ca^{2+} in stabilizing the highly charged $[TcO(OH)_5]^{3-}$ moiety.

The comprehensive thermodynamic model derived in the present work for the system Tc^{4+}–Na^+–Mg^{2+}–Ca^{2+}–H^+–Cl^-–OH^-–H_2O at T = 25 °C provides an accurate and robust tool for the calculation of Tc(IV) solubility in a diversity of geochemical conditions. This new thermodynamic model represents a significant improvement and is highly relevant for calculating reliable Tc(IV) source term concentrations in the context of safety assessments for nuclear waste repositories.

Acknowledgements

The authors would like to thank D. Fellhauer and A. Baumann (KIT–INE) for their support in the Pitzer calculations and technical assistance, respectively. The contribution of M. Böttle, E. Soballa and S. Heck (KIT–INE) to ICP–OES, SEM–EDS and TG–DTA analyses is highly appreciated. This work was funded by the German Federal Ministry of Economics and Technology (BMWi) under the project of VESPA.

References

1 J. A. Rard, M. H. Rand, G. Anderegg and H. Wanner, *Chemical thermodynamics of technetium*, Elsevier, North-Holland, Amsterdam, 1999.
2 V. Metz, H. Geckeis, E. Gonzalez-Robles, A. Loida, C. Bube and B. Kienzler, *Radiochim. Acta*, 2012, **100**, 699–713.
3 E. Wieland and L. R. Van Loon, *Cementitious Near-Field Sorption Data Base for Performance Assessment of an ILW Repository in Opalinus Clay*, PSI-Bericht 03-06, Nuclear Energy and Safety Research Department Laboratory for Waste Management, 2006.
4 C. Bube, V. Metz, E. Bohnert, K. Garbev, D. Schild and B. Kienzler, *Phys. Chem. Earth*, 2013, **64**, 87–94.
5 R. E. Meyer, W. D. Arnold, F. I. Case and G. D. Okelley, *Radiochim. Acta*, 1991, **55**, 11–18.
6 T. E. Eriksen, P. Ndalamba, J. Bruno and M. Caceci, *Radiochim. Acta*, 1992, **58-9**, 67–70.
7 N. J. Hess, Y. X. Xia, D. Rai and S. D. Conradson, *J. Solution Chem.*, 2004, **33**, 199–226.
8 D. J. Liu, J. Yao, B. Wang, C. Bruggeman and N. Maes, *Radiochim. Acta*, 2007, **95**, 523–528.
9 P. Warwick, S. Aldridge, N. Evans and S. Vines, *Radiochim. Acta*, 2007, **95**, 709–716.
10 T. Kobayashi, A. C. Scheinost, D. Fellhauer, X. Gaona and M. Altmaier, *Radiochim. Acta*, 2013, **101**, 323–332.
11 E. Yalcintas, X. Gaona, A. C. Scheinost, T. Kobayashi, M. Altmaier and H. Geckeis, *Radiochim. Acta*, 2015, **103**, 57–72.
12 L. Vichot, G. Ouvrard, G. Montavon, M. Fattahi, C. Musikas and B. Grambow, *Radiochim. Acta*, 2002, **90**, 575–579.
13 L. Vichot, M. Fattahi, C. Musikas and B. Grambow, *Radiochim. Acta*, 2003, **91**, 263–271.
14 F. Poineau, M. Fattahi, C. Den Auwer, C. Hennig and B. Grambow, *Radiochim. Acta*, 2006, **94**, 283–289.
15 F. Poineau, M. Fattahi and B. Grambow, *Radiochim. Acta*, 2006, **94**, 559–563.
16 F. Poineau, M. Fattahi and B. Grambow, *Radiochim. Acta*, 2006, **94**, 91–95.
17 F. Poineau, M. Fattahi, G. Montavon and B. Grambow, *Radiochim. Acta*, 2006, **94**, 291–299.
18 R. Guillaumont, T. Fanghänel, V. Neck, J. Fuger, D. A. Palmer, I. Grenthe and M. H. Rand, *Update on the chemical thermodynamics of uranium, neptunium, plutonium, americium and technetium*, Elsevier, North-Holland, Amsterdam, 2003.
19 B. Gorski and H. Koch, *J. Inorg. Nucl. Chem.*, 1969, **31**, 3565–3573.
20 M. Altmaier, V. Metz, V. Neck, R. Muller and T. Fanghänel, *Geochim. Cosmochim. Acta*, 2003, **67**, 3595–3601.
21 M. Altmaier, V. Neck and T. Fanghänel, *Radiochim. Acta*, 2008, **96**, 541–550.
22 M. Altmaier, V. Neck and T. Fanghänel, *Radiochim. Acta*, 2004, **92**, 537–543.
23 T. Omori, Y. Muraoka and H. Suganuma, *J. Radioan. Nucl. Ch. Ar.*, 1994, **178**, 237–243.
24 R. Kopunec, F. N. Abudeab and S. Skraskova, *J. Radioanal. Nucl. Ch.*, 1998, **230**, 51–60.
25 JCPDS, USA (2001), 2001.
26 J. Rothe, S. Butorin, K. Dardenne, M. A. Denecke, B. Kienzler, M. Löble, V. Metz, A. Seibert, M. Steppert, T. Vitova, C. Walther and H. Geckeis, *Rev. Sci. Instrum.*, 2012, **83**, 043105.
27 B. Ravel and M. Newville, *J. Synchrotron Radiat.*, 2005, **12**, 537–541.
28 S. R. Langhoff, C. W. Bauschlicher, L. G. M. Pettersson and P. E. M. Siegbahn, *Chem. Phys.*, 1989, **132**, 49–58.
29 E. Breynaert, C. E. A. Kirschhock and A. Maes, *Dalton Trans.*, 2009, 9398–9401.

30 R. Polly, B. Schimmelpfennig, E. Yalcintas, X. Gaona and M. Altmaier, *Hydrolysis of Tc(IV) and formation of ternary Na/Ca-Tc(IV)-OH species in NaCl/$CaCl_2$ systems: a quantum chemical study*, Migration conference, Santa Fe, USA, 2015.
31 A. A. Müller, H. Bogge and E. Diemann, *Inorg. Chem. Commun.*, 2003, **6**, 52–53.
32 A. Müller, H. Bogge and E. Diemann, *Inorg. Chem. Commun.*, 2003, **6**, 329–329.
33 A. Lenz and L. Ojamae, *J. Phys. Chem. A*, 2006, **110**, 13388–13393.
34 V. Neck, M. Altmaier, T. Rabung, J. Lützenkirchen and T. Fanghänel, *Pure Appl. Chem.*, 2009, **81**, 1555–1568.
35 D. Fellhauer, V. Neck, M. Altmaier, J. Lützenkirchen and T. Fanghänel, *Radiochim. Acta*, 2010, **98**, 541–548.
36 B. Brendebach, M. Altmaier, J. Rothe, V. Neck and M. A. Denecke, *Inorg. Chem.*, 2007, **46**, 6804–6810.
37 I. Almahamid, J. C. Bryan, J. J. Bucher, A. K. Burrell, N. M. Edelstein, E. A. Hudson, N. Kaltsoyannis, W. W. Lukens, D. K. Shuh, H. Nitsche and T. Reich, *Inorg. Chem.*, 1995, **34**, 193–198.
38 E. E. Rodriguez, F. Poineau, A. Llobet, A. P. Sattelberger, J. Bhattacharjee, U. V. Waghmare, T. Hartmann and A. K. Cheetham, *J. Am. Chem. Soc.*, 2007, **129**, 10244–10248.
39 G. H. Morrison and H. Freiser, *Solvent Extraction in Analytical Chemistry*, John Willey & Sons, Inc., London, 1957.
40 J. C. Shannon, *Database of ionic radii*, http://abulafia.mt.ic.ac.uk/shannon/ptable.php.
41 H. Wanner, *Guidelines for the assignment of uncertainties*, Elsevier, F-92130 Issy-les-Moulineaux, France, 1999.
42 W. Hummel, *Ionic strength corrections and estimation of SIT ion interaction coefficients*, Paul Scherrer Institut, 2009.
43 C. E. Harvie, N. Moller and J. H. Weare, *Geochim. Cosmochim. Acta*, 1984, **48**, 723–751.
44 I. Grenthe and I. Puigdomenech, *Modelling in aquatic chemistry*, Elsevier, Paris, 1997.
45 H. Gamsjäger, T. Gajda, J. Sanster, S. K. Saxena and W. Voigt, *Chemical thermodynamics of tin*, Elsevier, Issy-les-Moulineaux (France), 2012.
46 D. Fellhauer, PhD, University of Heidelberg, 2013.
47 D. Fellhauer, M. Altmaier, X. Gaona, J. Lützenkirchen and T. Fanghänel, *Radiochim. Acta*, 2016, DOI: 10.1515/ract-2015-2490.
48 V. Neck, T. Fanghänel and J. Kim, *Thermodynamische Modellierung von Technetium in Natürlichen Aquatischen Systemen*, FZKA 6340, Forschungszentrum Karlsruhe, Germany, 1999.